cancers

MDPI

Article

Colorectal Cancer Progression Is Potently Reduced by a Glucose-Free, High-Protein Diet: Comparison to Anti-EGFR Therapy

Kerstin Skibbe [1,†], Ann-Kathrin Brethack [1,†], Annika Sünderhauf [1], Mohab Ragab [1], Annika Raschdorf [1], Maren Hicken [1], Heidi Schlichting [1], Joyce Preira [1], Jennifer Brandt [1], Darko Castven [2], Bandik Föh [1], René Pagel [3], Jens U. Marquardt [2], Christian Sina [1,4] and Stefanie Derer [1,*]

1 Institute of Nutritional Medicine, University Hospital Schleswig-Holstein, Campus Lübeck, 23538 Lübeck, Schleswig-Holstein, Germany; kerstin.skibbe@gmail.com (K.S.); annkathrin.brethack95@gmail.com (A.-K.B.); annika.suenderhauf@uksh.de (A.S.); mohab.ragab@uksh.de (M.R.); annika.raschdorf@uksh.de (A.R.); maren.hicken@uksh.de (M.H.); heidi.schlichting@uksh.de (H.S.); joyce.preira@icloud.com (J.P.); jennifer.brandt@student.uni-luebeck.de (J.B.); bandik.foeh@uksh.de (B.F.); Christian.Sina@uksh.de (C.S.)
2 1st Department of Medicine, University Hospital Schleswig-Holstein, Campus Lübeck, 23538 Lübeck, Schleswig-Holstein, Germany; darko.castven@uksh.de (D.C.); Jens.Marquardt@uksh.de (J.U.M.)
3 Institute of Anatomy, University of Lübeck, 23538 Lübeck, Schleswig-Holstein, Germany; pagel@anat.uni-luebeck.de
4 1st Department of Medicine, Division of Nutritional Medicine, University Hospital Schleswig-Holstein, Campus Lübeck, 23538 Lübeck, Schleswig-Holstein, Germany
* Correspondence: stefanie.derer@uksh.de
† These authors contributed equally to this study.

Simple Summary: To study the interplay between nutrition and intestinal metabolism in the context of colitis-driven colorectal carcinoma (CRC), we here investigated a nutritional therapy strategy in the presence or absence of EGFR-directed antibody therapy in mice to treat established colitis-driven CRCs in vivo. After CRC development, mice were fed a control diet or an isoenergetic glucose-free high-protein (GFHP) diet in the presence or absence of EGFR-directed antibody therapy. The GFHP diet was accompanied by a metabolic shift of the mice towards lower glycolysis activity. Both, GFHP diet or anti-EGFR antibody treatment, improved tumor differentiation and anti-tumor immune response, resulting in an efficient reduction of colonic tumor burden.

Abstract: To enable rapid proliferation, colorectal tumor cells up-regulate epidermal growth factor receptor (EGFR) signaling and aerobic glycolysis, resulting in substantial lactate release into the tumor microenvironment and impaired anti-tumor immune responses. We hypothesized that a nutritional intervention designed to reduce aerobic glycolysis may boost the EGFR-directed antibody (Ab)-based therapy of pre-existing colitis-driven colorectal carcinoma (CRC). CRC development was induced by azoxymethane (AOM) and dextran sodium sulfate (DSS) administration to C57BL/6 mice. AOM/DSS-treated mice were fed a glucose-free, high-protein diet (GFHPD) or an isoenergetic control diet (CD) in the presence or absence of an *i.p.* injection of an anti-EGFR mIgG2a or respective controls. AOM/DSS-treated mice on a GFHPD displayed a reduced systemic glucose metabolism associated with reduced oxidative phosphorylation (OXPHOS) complex IV expression and diminished tumor loads. Comparable but not additive to an anti-EGFR-Ab therapy, the GFHPD was accompanied by enhanced tumoral goblet cell differentiation and decreased colonic PD-L1 and splenic CD3ε, as well as PD-1 immune checkpoint expression. In vitro, glucose-free, high-amino acid culture conditions reduced proliferation but improved goblet cell differentiation of murine and human CRC cell lines MC-38 and HT29-MTX in combination with down-regulation of PD-L1 expression. We here found GFHPD to systemically dampen glycolysis activity, thereby reducing CRC progression with a similar efficacy to EGFR-directed antibody therapy.

Keywords: EGFR; colorectal cancer; amino acid metabolism; PD-L1; PD-1; AOM/DSS; goblet cell differentiation

Citation: Skibbe, K.; Brethack, A.-K.; Sünderhauf, A.; Ragab, M.; Raschdorf, A.; Hicken, M.; Schlichting, H.; Preira, J.; Brandt, J.; Castven, D.; et al. Colorectal Cancer Progression Is Potently Reduced by a Glucose-Free, High-Protein Diet: Comparison to Anti-EGFR Therapy. *Cancers* **2021**, *13*, 5817. https://doi.org/10.3390/cancers13225817

Academic Editors: Anna Dubrovska, Verena Jendrossek and Leoni Kunz-Schughart

Received: 22 October 2021
Accepted: 17 November 2021
Published: 19 November 2021

1. Introduction

Colorectal carcinoma (CRC) is one of the most common cancer entities worldwide, responsible for more than one million new cases annually [1]. The overall five-year survival rate is about 70%, with a recurrence rate of about 5% [2]. It is known that, in addition to genetic predisposition, various aspects of lifestyle, e.g., physical activity, alcohol consumption, nutrition, and smoking, are important risk factors [3,4]. Increasing evidence further suggests that chronic inflammation plays a crucial role in the pathogenesis of colorectal cancer [5,6]. Inflammatory bowel diseases (IBD), such as ulcerative colitis (UC) or Crohn's disease (CD), are examples of the link between inflammation and tumorigenesis, which is a potent risk factor for the development of colorectal cancer [7]. However, the underlying mechanisms remain elusive.

The epidermal growth factor receptor (EGFR) belongs to a family of transmembrane tyrosine kinase receptors. Because of its importance for tumor development and progression, the EGFR has long been considered as a promising target molecule for tumor therapy [8,9]. Overexpression or mutations of the EGFR are found in a variety of epithelial tumors such as CRC [10]. Therapeutically, EGFR can be targeted by small-molecule tyrosine kinase inhibitors (e.g., erlotinib and gefitinib) or by monoclonal antibodies (mAbs) [8]. Currently, three monoclonal antibodies (cetuximab, panitumumab, and necitumumab) have been approved for therapeutic applications, but many more are in clinical development [11]. Approved indications include Kirsten rat sarcoma virus (KRAS), wild-type colon cancer for cetuximab and panitumumab, and head and neck cancer, where only cetuximab has been approved so far, as well as non-small cell lung cancer [12]. In contrast to EGFR blockade in cancer, the rectal application of EGF-containing enemas to ulcerative colitis patients induced mucosal healing in 10 out of 12 patients, highlighting the crucial role of the EGFR signaling cascade in intestinal epithelial regeneration. However, due to the potential activation of pro-oncogenic signaling pathways, this therapeutic strategy was not followed up [13]. In experimental murine colitis models, blockade of EGFR by the tyrosine kinase inhibitor gefitinib [14] or knockout of the EGFR [15] resulted in exacerbated colitis and colitis-driven colorectal carcinoma, indicating a crucial role of EGFR signaling cascades in intestinal tissue homeostasis. However, blockade of EGFR by the tyrosine kinase inhibitor gefitinib in mice displaying established colorectal tumors seemed to decrease polyp sizes, pointing to opposing roles of EGFR signaling in the resolution of intestinal inflammation and tumor growth [14].

A hallmark of cancer cells is increased glycolysis under normoxic conditions. In contrast to quiescent differentiated cells, tumor cells produce large amounts of lactate instead of CO_2 during glucose metabolism in the presence of oxygen [16,17], called "aerobic glycolysis". This metabolic switch was first described in 1923 by the German biochemist Otto Heinrich Warburg and is also known under the term "Warburg effect" [16]. With a sufficient supply of glucose and oxygen, 85% of the glucose in tumor cells enters aerobic glycolysis, a metabolic pathway that enables fast and direct accessible energy [18], while 5% of imported glucose is metabolized via oxidative phosphorylation (OXPHOS) using the mitochondrial respiratory chain [19]. The altered metabolism of a cancer cell is not only used to generate energy in the form of ATP [20], but the intermediates of glycolysis can be diverted into biosynthetic pathways to produce compounds for cell division [21]. Hence, recent studies showed that administration of 2-deoxy-D-glucose (2-DG), a glycolysis inhibitor, reduces the growth of colorectal carcinoma in mice [22].

In triple-negative breast cancer cells, it has been shown that the EGFR signal activates the first step of glycolysis. At the same time, however, this signal also inhibits the last step of glycolysis, resulting in an accumulation of metabolic intermediates such as fructose-1,6-bisphosphate (F1,6BP). The latter enhances its action by directly binding to the EGFR, thereby increasing lactate excretion. Increased lactate production, in turn, leads to an inhibition of local cytotoxic T cells and a reduced anti-tumor immune response [23].

To date, only two antibodies against the murine EGFR (mEGFR) are known, the 7A7 [24] and another antibody produced by ImClone [25]. Previous studies show that the so-called 7A7 antibody (7A7-Ab) recognizes the extracellular domain of the mEGFR on healthy cells and tumor cells. In addition, 7A7-Ab inhibited the EGF-induced signaling cascade of the EGFR in the murine lung carcinoma cell line 3LL-D122 [26,27]. The inhibition of EGFR-mediated signal transduction induced apoptosis, thereby evoking the initiation of anti-tumor immune responses.

Considering that an acidic tumor microenvironment crucially impairs immune effector cell activation and therefore anti-tumor immune responses [28], we hypothesized that the efficacy of EGFR-targeting antibody-based therapy can be increased by metabolic reprogramming of the tumor itself. Hence, we here investigated the therapeutic efficacy of an optimized nutritional intervention designed to inhibit increased aerobic glycolysis of tumor cells in the presence or absence of an EGFR-directed antibody-based therapy in a mouse model of colitis-driven CRC. Therefore, we applied the sporadic azoxymethane (AOM)/dextran sodium sulfate (DSS) triggered mouse model of colitis-driven colorectal cancer [29,30]. AOM is a genotoxic carcinogen that causes DNA damage and tumorigenesis, and it specifically induces the development of colorectal cancer in rodents [31]. The combination of AOM with the inflammatory drug DSS is widely used in colitis-driven colon carcinogenesis in mouse models [32].

2. Results

2.1. Anti-EGFR Ab Therapy or Glucose-Free, High-Protein Nutritional Intervention Efficaciously Prevents CRC Progression

To study the effect of a nutritional intervention in the presence or absence of anti-EGFR Ab treatment on the progression of pre-existing CRC in mice, we first induced sporadic colitis-driven CRC in C57BL/6 mice until day 70 by intraperitoneal (*i.p.*) injection of 10 mg/kg/body weight (BW) AOM at day zero and a second *i.p.* injection of 5 mg/kg/BW AOM at day 21. Colitis was induced by the application of 2% (*w*/*v*) DSS via the drinking water between day 7 and 14 and was boosted by a second application of 1% (*w*/*v*) DSS via the drinking water between day 42 and 45. C57BL/6 control mice underwent *i.p.* injections of 1× PBS instead of AOM and remained on normal drinking water (Figure 1a). Before in vivo application, we studied the binding of utilized monoclonal murine IgG2a antibody 7A7 (anti-EGFR Ab) to the murine recombinant EGFR protein by ELISA experiments and determined a significant, concentration-dependent binding, while the control antibody CD19-mIgG2a (ctrl. Ab) did not show any binding capacity to murine EGFR (Figure 1b). During the first 70 days, the disease activity index (DAI), combining weight loss, stool consistency, and rectal bleeding, was monitored every two days, and it indicated successful colitis induction in AOM/DSS-treated mice in comparison to PBS control mice (Figure 1c). On day 70, indicator mice were sedated and endoscopically examined before sacrificing. As presented in Figure 1d, AOM/DSS-treated mice displayed colorectal tumor development, while no tumors were endoscopically detected in PBS-treated mice at day 70 (Figure 1d). As expected from human CRC studies, increased *Egfr* mRNA expression and EGFR protein levels were detected in colorectal tumors from AOM/DSS-treated mice in comparison to normal tissue (Figure 1e).

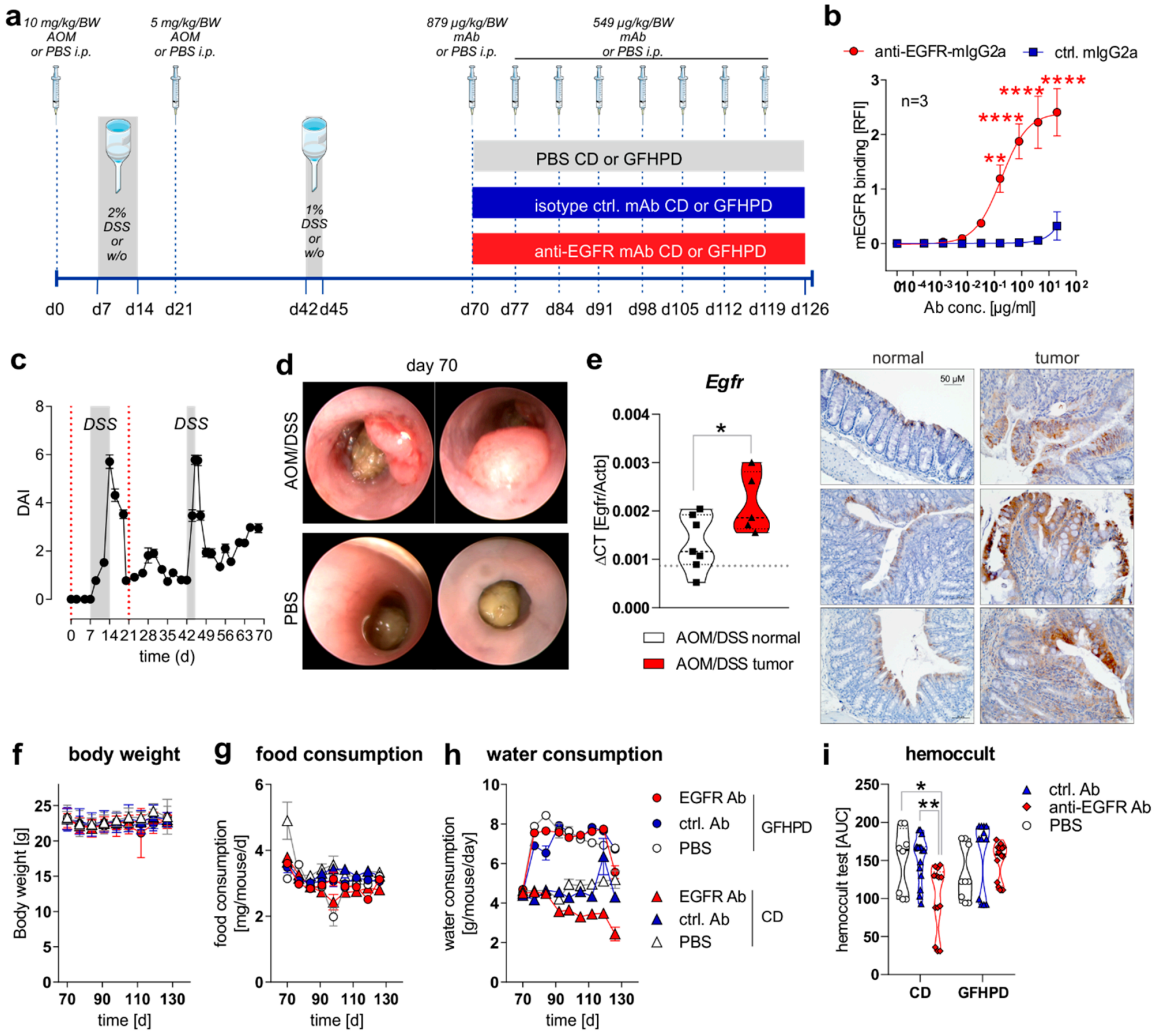

Figure 1. EGFR expression is elevated in CRC tumors and anti-EGFR Ab treatment reduces fecal occult blood levels in AOM/DSS-treated mice. (**a**) Schematic overview of induction of colitis-driven colorectal carcinomas by AOM/DSS treatment in female C57BL/6J mice (n = 88) between days 0 and 70. Control mice received PBS instead of AOM/DSS (n = 19) between days 0 and 70. At day 70, indicator mice (n = 9 AOM/DSS-treated; n = 8 PBS-treated) were sacrificed and tissues were sampled for further analysis. Remaining AOM/DSS-treated mice were further subdivided at day 70 into two different dietary intervention groups receiving control diet (CD; n = 39) or glucose-free, high-protein diet (GFHPD; n = 40) until day 126. Dietary interventions were performed in the presence or absence of weekly intraperitoneal (*i.p.*) application of PBS (n = 9 CD; n = 9 GFHPD), anti-EGFR Ab (n = 15 CD; n = 16 GFHPD) or a ctrl. antibody (n = 15 CD; n = 15 GFHPD) between day 70 and 126. PBS-treated control mice were fed either CD (n = 5) or GFHPD (n = 6) between day 70 and 126. AOM = azoxymethane; DSS = dextran sodium sulfate; anti-EGFR-mAb = 7A7-mIgG2a; isotype ctrl. mAb = irrelevant mIgG2a; mAb = monoclonal Ab. (**b**) Concentration-dependent binding of anti-EGFR-mIgG2a or ctrl.-mIgG2a to recombinant murine EGFR was analyzed by ELISA experiments. Mean ± SEM of three independent experiments is presented. (**c**) Disease activity index (DAI) of AOM/DSS-treated mice (n = 88) from day 0 to 70. (**d**) Representative images of endoscopy analyses of AOM/DSS or PBS-treated indicator mice at day 70. (**e**) *Egfr* mRNA expression was quantified by qPCR and related to *Actb* mRNA expression in normal or tumor colonic tissues collected from AOM/DSS-treated mice at day 70. Grey dotted line indicates median values of PBS-treated control mice at day 70 (left panel). Representative images of immunohistochemistry staining of EGFR in paraffin-embedded normal and tumor colonic biopsies (n = 3 each) were collected from AOM/DSS-treated mice at day 70 (right panel). Scale bar = 50 µM. (**f**–**h**) Body weight, food consumption, and water consumption were routinely monitored between days 70 and 126. (**i**) Fecal occult blood was determined every second day using a hemoccult test. Results are presented as the area under the curve (AUC) from analyzed mice. * $p \leq 0.05$, ** $p \leq 0.01$. **** $p \leq 0.0001$.

From day 70 on, AOM/DSS-treated or PBS-treated mice were separated into two subgroups, with one group receiving a control diet (CD; 22% protein/casein, 14% fat, 64% carbohydrates; Table 1) and one receiving an isoenergetic glucose-free, high-protein diet (GFHPD; 66% protein/casein, 32% fat, 2% carbohydrates w/o glucose; Table 1) as a therapeutic regimen. Furthermore, AOM/DSS-treated mice either in CD or GFHPD groups additionally received an initial dose of 0.879 mg/kg/BW of anti-EGFR Ab, ctrl. Ab, or PBS at day 70 and a weekly dose of 0.563 mg/kg/BW from day 77 until day 126 by *i.p.* injection (Figure 1a). Regularly, body weight and food and water consumption, as well as fecal blood, were determined to monitor the health status of all analyzed mice. While no differences were observed between nutritional intervention and antibody treatment groups regarding body weight (Figure 1f) and food consumption (Figure 1g), all mice on the GFHD, irrespective of antibody treatment, displayed significantly increased water consumption in comparison to CD mice (Figure 1h). Of note, the hemoccult test revealed anti-EGFR Ab treatment to significantly decrease the frequency of fecal blood in CD but not in GFHPD-fed AOM/DSS-treated mice compared to PBS or ctrl. Ab-treated mice (Figure 1i).

Table 1. Chow composition as provided by the manufacturer.

Diet Composition	Isoenergetic Control Diet	Glucose Free High Protein Diet
Casein	20%	60%
Brewer's yeast	-	2%
Corn starch	28%	-
Maltodextrin	14.5%	-
Sucrose	10%	-
Cellulose powder	15%	19.5%
L-Cystine	0.3%	0.3%
Vitamin premixture	1%	1%
Minerals and trace elements	6%	6%
Choline chloride	0.2%	0.2%
Soybean oil	5%	11%
Crude protein	17.7%	53.4%
Crude fat	5.1%	11.4%
Crude fiber	15.8%	20.3%
Crude ash	5.4%	5.9%
Starch	26.9%	0.1%
Sugar	9.9%	-
NfE	51.7%	1.9%
Physiological fuel value	13.6 MJ/kg	13.6 MJ/kg
Protein	22 kcal%	66 kcal%
Fat	14 kcal%	32 kcal%
Carbohydrates	64 kcal%	2 kcal%

NfE: nitrogen-free extract.

As expected, in AOM/DSS-treated mice on CD, anti-EGFR Ab treatment markedly lowered the frequency of large tumors with a score of 5 compared to ctrl. Ab (ctrl. Ab = 50% of tumors with a tumor score of 5, anti-EGFR Ab = 22.2% of tumors with tumor score of 5). Similarly, the application of an anti-EGFR Ab to AOM/DSS-treated mice fed a GFHPD significantly reduced the presence of large tumors with a tumor score of 5 (27.3%) when compared to ctrl. Ab application (57.1%), resulting in a higher percentage of tumors with a tumor score of 4 (27.3%), while no tumors with a tumor score of 4 were detected in GFHPD-fed mice treated with the ctrl. Ab. Compared to CD, GFHPD did not alter the presence of large colonic tumors of tumor score 5 in AOM/DSS and ctrl. Ab-treated mice. However, consumption of a GFHPD by AOM/DSS and ctrl. Ab-treated mice lowered the presence of colonic tumors with a score between 1–4, therefore increasing the percentage of tumor-free mice to 43% in comparison to 20% tumor-free mice in the CD group (Figure 2a,b). Results received from tumor scoring analyses were reflected by endoscopic examination of the colon that indicated a significantly reduced murine endoscopic index of colitis severity (MEICS) in AOM/DSS and ctrl. Ab-treated mice fed a GFHPD (mean ± SD; 1.8 ± 1.2) in comparison to CD (mean ± SD; 4.1 ± 1.7). While anti-EGFR Ab treatment resulted in a trend towards a reduced MEICS score (mean ± SD; 2.9 ± 2.2) in AOM/DSS mice fed a CD in comparison to ctrl. Ab treatment, the MEICS score was slightly increased, but without statistical significance, by the anti-EGFR Ab treatment in AOM/DSS mice fed a GFHPD (mean ± SD; 3.2 ± 1.4) (Figure 2c).

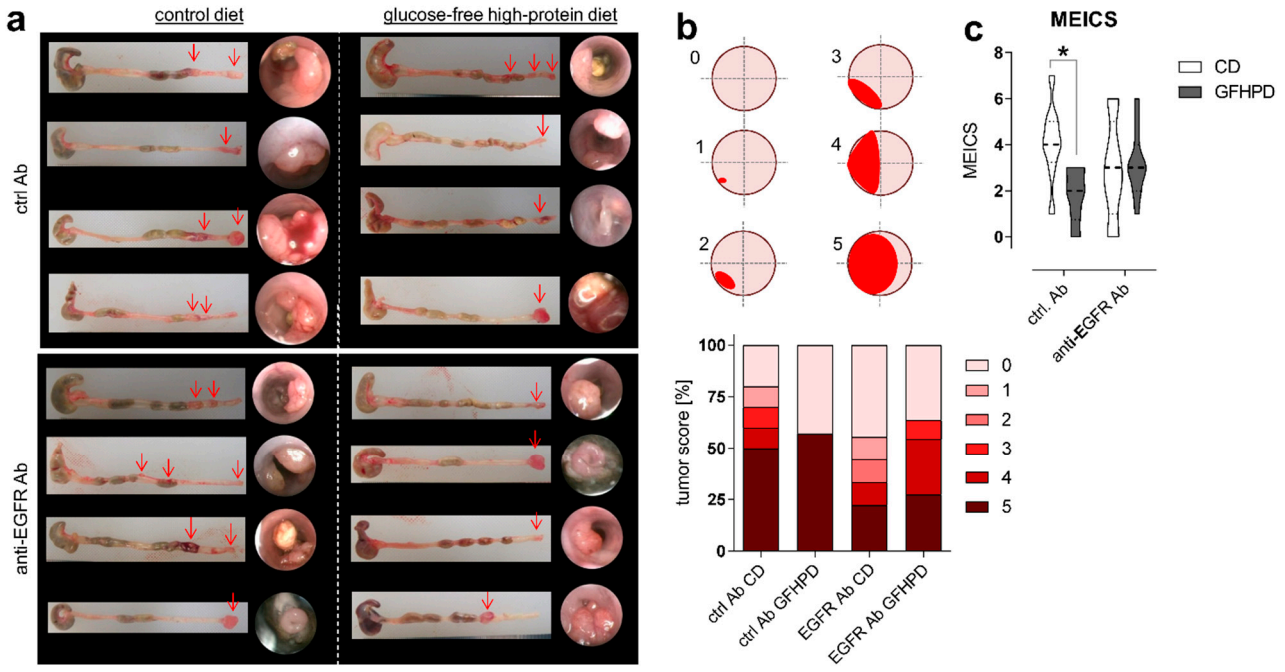

Figure 2. GFHPD displays comparable efficacy in CRC tumor load reduction in comparison to anti-EGFR Ab treatment. (**a**) Representative images (n = 4 per indicated group) from colons collected from AOM/DSS-treated mice and respective endoscopic analysis at day 126. (**b**) Colorectal tumors were scored between 0 and 5 as described in [33]. Percentages for each tumor score were calculated per treatment group. (**c**) Murine endoscopic index of colitis severity (MEICS) was determined according to [33]. * $p \leq 0.05$.

2.2. A Glucose-Free, High-Protein Diet Increases Amino Acid Metabolism and Decreases Lactate and Insulin Production

To investigate the effect of GFHPD consumption on systemic and colonic metabolisms in AOM/DSS-treated mice, we analyzed metabolic markers in serum and colonic biopsy samples collected at day 126 from ctrl. Ab or anti-EGFR Ab-treated mice. Here, in ctrl. Ab-treated mice, L-lactate serum levels were found to be significantly reduced in GFHPD-fed mice in comparison to CD-fed mice, while no alterations were detected after anti-EGFR Ab therapy (Figure 3a). Of note, comparable glucose serum levels were determined in all analyzed groups (Figure 3b), while GFHPD lowered insulin levels without reaching statistical significance in ctrl. Ab-treated mice (mean ± SD, 2.8 ± 6.3 µiU/mL) when compared to CD-fed mice (mean ± SD, 6.9 ± 6.1 µiU/mL; Figure 3c).

In line with insulin serum levels, C-peptide serum levels were significantly reduced in ctrl. Ab-treated mice fed a GFHPD (Figure 3d). Furthermore, anti-EGFR Ab therapy in CD-fed mice did not alter insulin or C-peptide serum levels in comparison to ctrl. Ab treatment, while GFHPD-fed mice showed reduced insulin but increased C-peptide serum levels after anti-EGFR Ab therapy (mean ± SD, 0.7 ± 3.1 µiU/mL) compared to ctrl. Ab-treated mice (Figure 3c,d). As an expected physiological reaction to high protein consumption, branched-chain amino acid and L-alanine serum levels were significantly enhanced in ctrl. Ab-treated mice fed a GFHPD compared to a CD, while no alterations were observed in all other treatment groups (Figure 3e,f). Due to the significantly elevated water consumption and serum amino acid load in GFHPD-fed mice, we studied kidney morphologies in order to exclude kidney failure. Here, no microscopic signs of kidney injury could be detected by HE staining analysis in any analyzed group (Figure 3g).

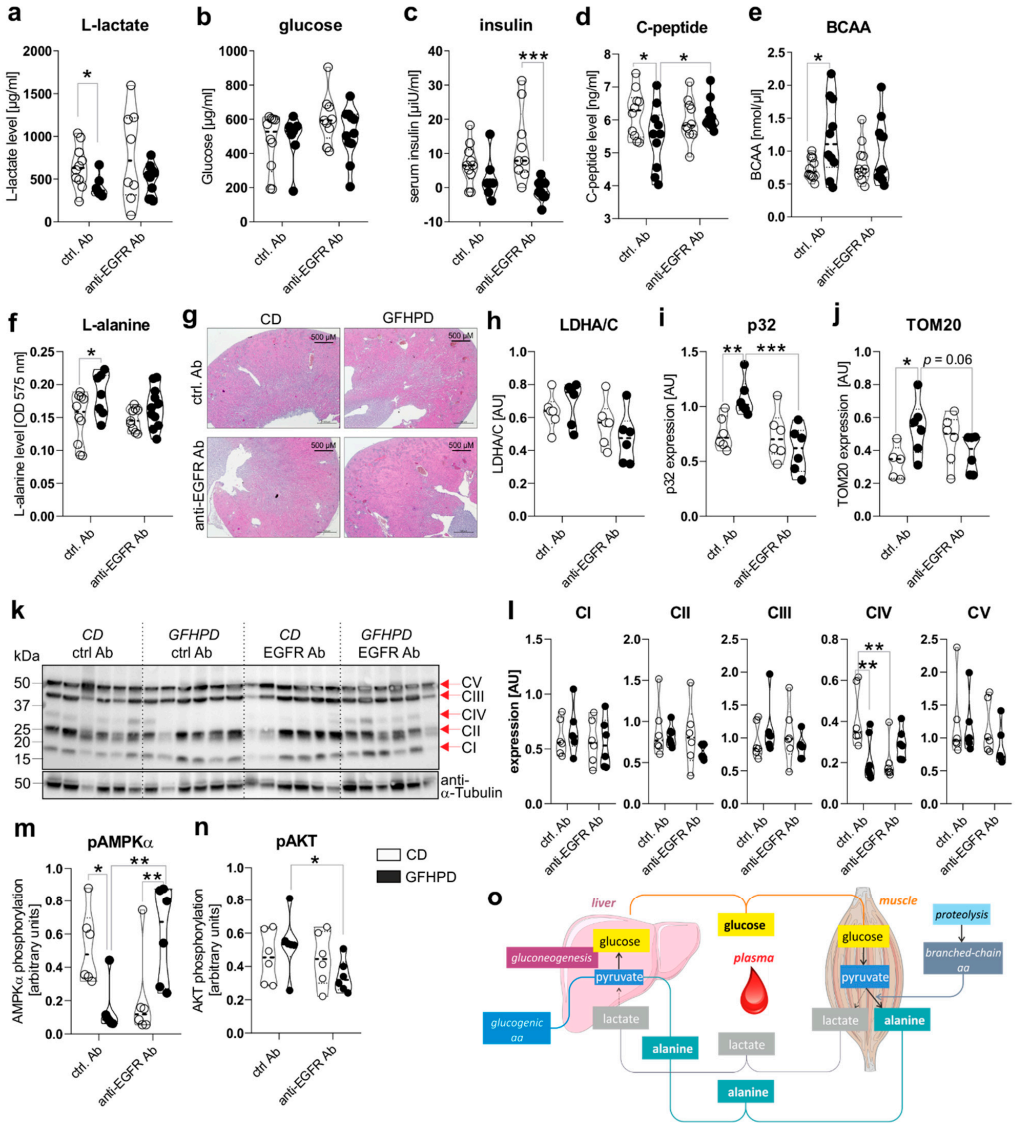

Figure 3. GFHPD application induces a metabolic shift from glycolysis towards amino acid metabolism and reduces colonic energy supply in AOM/DSS-treated mice. (**a**–**f**) Serum samples collected from indicated treatment groups at day 126 were analyzed with regard to (**a**) L-lactate, (**b**) D-glucose, (**c**) insulin, (**d**) C-peptide, (**e**) branched-chain amino acids (BCAA), or (**f**) L-alanine. ctrl. Ab (n = 10 CD; n = 7–10 GFHPD), anti-EGFR Ab (n = 8–10 CD; n = 9–11 GFHPD). (**g**) Representative images of HE-stained kidney tissue collected at day 126 from indicated treatment groups of AOM/DSS tumor mice. Original magnification, 2.5×. (**h**–**n**) Protein expression of (**h**) LDHA/C, (**i**) p32, (**j**) TOM20, (**k**,**l**) OXPHOS complexes I–V, (**m**) phosphorylated AMPKα, (**n**) phosphorylated AKT, or α-Tubulin was determined by Western blot experiments utilizing biopsy samples collected from colorectal tumors (n = 6 per group) of indicated treatment groups at day 126. Densitometric analysis was performed using ImageJ software and data were normalized to α-Tubulin values. (**o**) Schematic overview of systemic amino acid metabolism. * $p \leq 0.05$, ** $p \leq 0.01$. *** $p \leq 0.001$. AU = arbitrary units.

In the next set of experiments, we investigated the impact of increased systemic amino acid and decreased glucose metabolism on the colonic metabolism. Therefore, we performed Western blot experiments utilizing colonic biopsy samples from AOM/DSS and ctrl. Ab or anti-EGFR Ab-treated mice fed a CD or a GFHPD. Despite the decreased systemic glucose metabolism in GFHPD mice, no alterations in colonic lactate dehydrogenase a/c (LDHA/C) protein expression could be observed between all four groups (Figure 3h). Of note, expression of mitochondrial markers such as p32 (Figure 3i) and translocase of outer mitochondrial membrane 20 (TOM20; Figure 3j) was significantly increased in AOM/DSS and ctrl. Ab-treated mice fed a GFHPD when compared to CD feeding, revealing the

GFHPD to boost mitochondrial mass. Furthermore, the enhanced expression of mitochondrial markers p32 and TOM20 in ctrl. Ab-treated mice was significantly down-regulated in anti-EGFR Ab-treated mice under GFHPD. To study mitochondrial OXPHOS activity, we investigated colonic expression and assembly of OXPHOS complexes I-V in the analyzed mice by Western blot experiments. Of note, we utilized a cocktail of antibody clones that are specific for a subunit of each OXPHOS complex that is labile when its complex is not assembled, thereby indicating correct assembly of the complexes. As depicted in Figure 3, no differences in expression were observed for complexes I–III and V between the analyzed groups. Notably, the expression of complex IV, the cytochrome c oxidase, was significantly reduced in AOM/DSS and anti-EGFR Ab-treated mice fed a CD, as well as in AOM/DSS and ctrl. Ab-treated mice fed a GFHPD (Figure 3k,l).

Reduced complex IV expression is associated with a loss of mitochondrial OXPHOS activity, ATP production, and cell proliferation [34]. Additionally, complex IV constitutes the main regulation site of OXPHOS [35]. Reduced OXPHOS complex IV assembly in GFHPD-fed and ctrl. Ab-treated mice, as well as in CD-fed and anti-EGFR Ab-treated mice, was associated with a reduction of AMPKα phosphorylation that was again elevated under anti-EGFR Ab treatment in GFHPD-fed mice (Figure 3m). Due to the capacity of the activated AKT pathway to regulate AMPKα activation, especially under metabolic stress conditions [36], we further analyzed activation of the colonic AKT signaling pathway in AOM/DSS-treated mice by Western blot experiments. Although we detected significantly decreased colonic pAMPKα levels in AOM/DSS mice treated either with GFHPD plus ctrl. Ab or with CD plus anti-EGFR Ab (Figure 3m), phosphorylation of AKT was not altered in these mice but was reduced in anti-EGFR Ab-treated mice fed a GFHPD (Figure 3n), pointing to no antagonistic function of the AKT pathway onto the AMPKα pathway in the analyzed samples.

To conclude, metabolic analyses of AOM/DSS mice indicate that a GFHP nutritional intervention in contrast to a control diet reduces systemic glucose metabolism and increases amino acid metabolism to maintain a constant glucose serum level (Figure 3o). Furthermore, GFHPD consumption, as well as anti-EGFR Ab treatment, seems to be associated with a low-energetic colonic metabolism evoked by a loss of OXPHOS activity, resulting in inhibition of CRC progression in mice.

2.3. Goblet Cell Differentiation Is Enhanced by GFHP Diet or anti-EGFR Ab Therapy in AOM/DSS-Treated Mice

Cell proliferation and differentiation processes in the colon are driven by caspase-1 mediated metabolic switches between aerobic glycolysis and mitochondrial OXPHOS activity, respectively, and need to be tightly controlled to maintain proper colonic barrier function [37,38]. Due to findings from the metabolic analyses presented in Figure 3, we further investigated mRNA expression levels of *Caspase-1* as well as colonic epithelial cell differentiation markers *Lgr5*, *Hes1*, *Atoh1*, *Spdef1*, and *Klf4* (Figure 4a). Notably, no differences in colon length as a marker for colitis activity could be detected between all four analyzed treatment groups (Figure 4b), while *Caspase-1* mRNA was reduced ($p = 0.051$) in ctrl. Ab-treated and GFHPD-fed mice compared to CD mice (Figure 4c), pointing to decreased colonic cell proliferation under GFHPD. As depicted in Figure 4d–g, we did not detect any differences between analyzed mice in mRNA expression of the intestinal stem cell marker *Lgr5* (Figure 4d), the enterocyte marker *Hes1* (Figure 4e), the secretory cell precursor marker *Atoh1* (Figure 4f), and the goblet cell precursor marker *Spdef1* (Figure 4g). In line with reduced mRNA expression of the intestinal cell proliferation mediator *Caspase-1*, we found a significantly increased mRNA expression of the goblet cell differentiation markers *Klf4* and *Muc2* in GFHPD-fed vs. CD-fed AOM/DSS mice that were treated with a ctrl. Ab. Furthermore, *Klf4* mRNA expression was also significantly increased in anti-EGFR Ab vs. ctrl. Ab-treated mice fed a CD, while *Muc2* expression was significantly reduced in anti-EGFR Ab vs. ctrl. Ab-treated mice fed a GFHPD (Figure 4h,i).

For validation of the qPCR data, we performed histochemical staining experiments. Here, increased neutral and acidic mucin expression was determined by PAS/Alcian blue

(Figure 4j, left panel) or Alcian blue (Figure 4j, right panel) staining of colonic tumors in either GFHPD-fed mice (ctrl. Ab or anti-EGFR Ab-treated) or in anti-EGFR Ab-treated mice fed a CD (Figure 4j). As a functional consequence of enhanced mucus production, we analyzed fecal C3 cleavage products that were previously shown to be triggered by Gram-negative mucosa-associated bacteria via Toll-like receptor 4 (TLR4) signaling in intestinal epithelial cells and hence to constitute a fecal marker of intestinal barrier integrity [39]. While colonic *C3* mRNA expression did not differ between analyzed groups (Figure 4k, left panel), fecal C3b/d/g protein levels were significantly decreased in GFHPD-fed mice treated with a ctrl. Ab or in CD-fed mice treated with an anti-EGFR Ab in comparison to ctrl. Ab-treated mice fed a CD (Figure 4k, right panel). Fecal C3 cleavage products were not further reduced in GFHPD-fed mice plus anti-EGFR Ab therapy. Together, GFHPD consumption enhances colorectal goblet cell differentiation in AOM/DSS and ctrl. Ab-treated mice to a comparable extent as anti-EGFR Ab therapy, resulting in an improved intestinal barrier function.

2.4. Increased Amino Acid Metabolism Enhances Goblet Cell Differentiation in Colorectal Tumor Cells In Vitro

To mechanistically validate the described ex vivo results, in vitro experiments were performed utilizing the murine colorectal carcinoma cell line MC-38 and the human colorectal carcinoma cell line HT29-MTX. MC-38 cells were incubated for 72 h in culture media containing increasing concentrations of glucose (0–25 mM) in the presence of 1% non-essential amino acids (NEAA), 10% NEAA, or 20% NEAA to study cell proliferation, differentiation, and lactate production. In concordance with in vivo data, MC-38 cell viability was increased in a glucose-concentration-dependent manner that was further elevated in the presence of increasing NEAA concentrations (Figure 5a).

Of note, MC-38 cells that were cultivated in a glucose-free medium enriched with NEAA (1%, 10%, and 20%) displayed significantly decreased cell proliferation in comparison to the standard culture medium (25 mM glucose, 1% NEAA) (Figure 5b), as well as a reduced expression of mitochondrial OXPHOS complex II (no changes for complexes III and V) but an increased expression of the autophagy marker LC3B-II (Figure 5c,d), indicating a low-energetic metabolic state that may promote autophagy. Decreased cell proliferation of MC-38 cells under glucose-free plus 20% NEAA conditions after 48 h of cultivation was also reflected by decreased mRNA and protein expression of proliferation driving Caspase-1 (Figure 5e) and reduced activation of the main proliferation pathway via AKT (Figure 5f). Consistent with these findings, incubation of HT29-MTX cells under glucose-free plus 10% NEAA conditions also demonstrated significantly reduced cell proliferation in comparison to glucose-containing plus 1% NEAA conditions (Figure 5g). As we observed decreased lactate serum levels in AOM/DSS and ctrl. Ab-treated mice fed a GFHPD vs. CD, we measured the lactate release of MC-38 and HT29-MTX cells. Similar to cell proliferation results, the lactate release by MC-38 cells increased in a glucose-concentration-dependent manner after 72 h of incubation. While the highest lactate release was detected in MC-38 cells cultivated for 72 h in 25 mM glucose plus 1% NEAA containing medium, a lower one was achieved by the addition of 20% NEAA to the culture medium (Figure 5h). Likewise, under glucose-free culture conditions, the lactate release by MC-38 cells was lowest in the presence of 20% NEAA (Figure 5i). These results were validated in HT29-MTX cells that displayed significantly decreased lactate release per cell in glucose-free plus 10% NEAA culture conditions in comparison to 25 mM glucose plus 1% NEAA culture conditions (Figure 5j). To investigate whether decreased cell proliferation of CRC cell lines in glucose-free plus high amino acid conditions results in enhanced goblet cell differentiation, we studied goblet cell marker levels in MC-38 and HT29-MTX cells. Whereas mRNA expression of the goblet cell marker *Klf4* was not significantly altered by metabolic challenges in MC-38 cells, *Muc2* mRNA expression and Muc2 secretion were significantly increased under glucose-free plus 20% NEAA culture conditions when compared to 25 mM glucose plus 1% NEAA culture conditions after 48 h of incubation (Figure 5k). As expected, a significantly elevated Muc5AC release was observed in HT29-MTX cells

incubated for 72 h in glucose-free plus 10% NEAA culture conditions in comparison to cultivation under 25 mM glucose plus 1% NEAA (Figure 5l). In summary, reduced glucose metabolism and enhanced amino acid metabolism improves goblet cell differentiation in colorectal carcinoma cells.

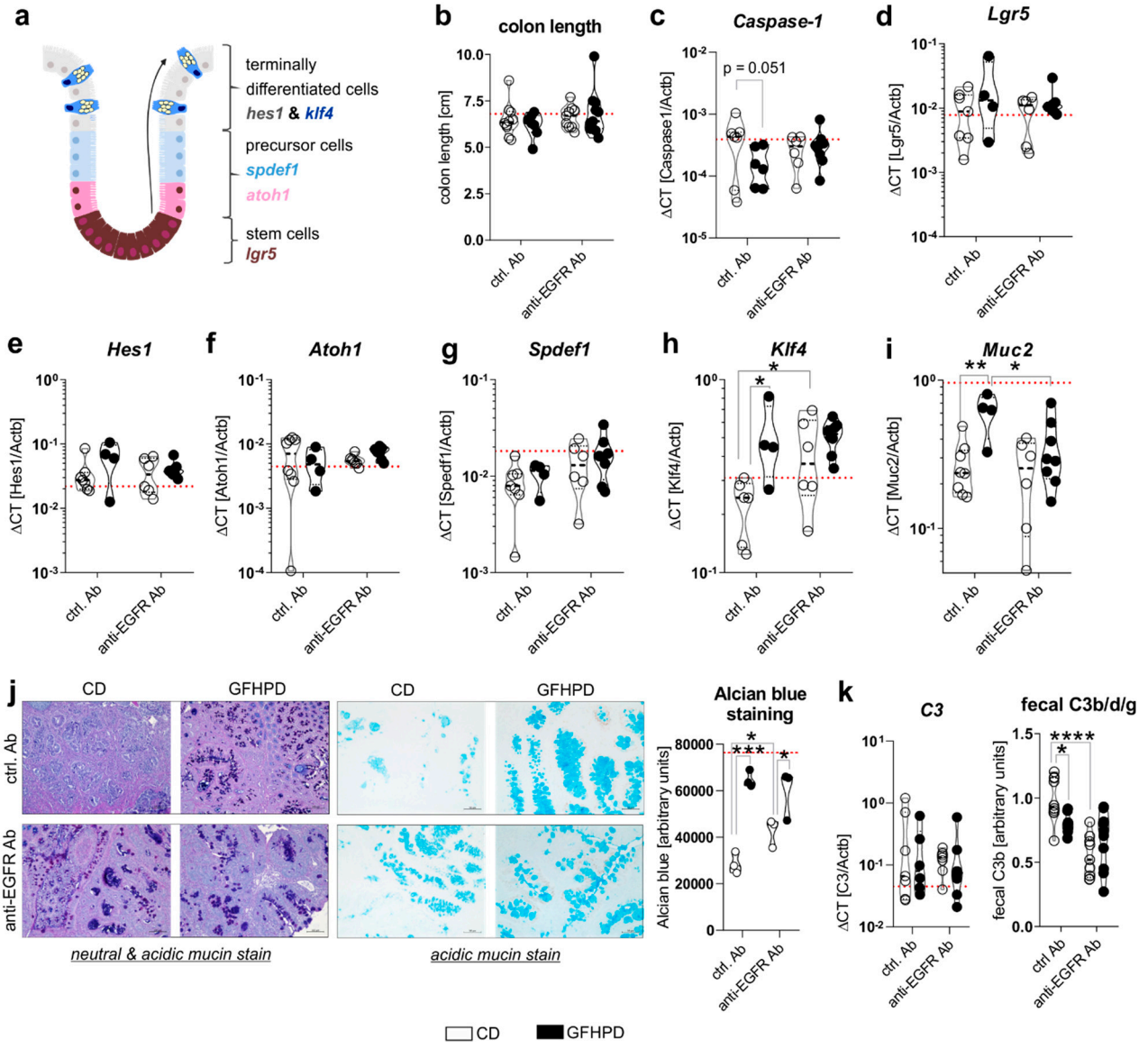

Figure 4. GFHPD consumption is accompanied by increased goblet cell differentiation of CRC tumors to a similar extent compared to anti-EGFR Ab therapy. (**a**) A model for intestinal epithelial cell differentiation in the colonic crypt. (**b**) Whole colon length was determined at day 126. (**c**–**i**) mRNA expression levels of (**c**) *Caspase-1*, (**d**) *Lgr5*, (**e**) *Hes1*, (**f**) *Atoh1*, (**g**) *Spdef1*, (**h**) *Klf4*, or (**i**) *Muc2* were quantified by qPCR in colonic biopsy samples collected from indicated treatment groups. Ctrl. Ab (n = 6–8 CD; n = 4–6 GFHPD), anti-EGFR Ab (n = 6–7 CD; n = 8–9 GFHPD). (**j**) Representative histochemical PAS/Alcian (left panel) or Alcian blue (right panel) staining of PFA-fixed, paraffin-embedded tumor tissue biopsies from indicated treatment groups. Original magnification, 10×. (**k**) Colonic *C3* mRNA expression was quantified by qPCR experiments (left panel). Ctrl. Ab (n = 7 CD; n = 6 GFHPD), anti-EGFR Ab (n = 7 CD; n = 8 GFHPD). Fecal C3b/d/g protein levels were measured by Western blot experiments utilizing fecal samples collected from indicated treatment groups of AOM/DSS mice (right panel). Densitometric analysis was performed using the ImageJ software. Ctrl. Ab (n = 10 CD; n = 7 GFHPD), anti-EGFR Ab (n = 9 CD; n = 10 GFHPD). Red dotted horizontal lines represent respective median values of PBS-treated control mice at day 126. * $p \leq 0.05$, ** $p \leq 0.01$, *** $p \leq 0.001$, **** $p \leq 0.0001$.

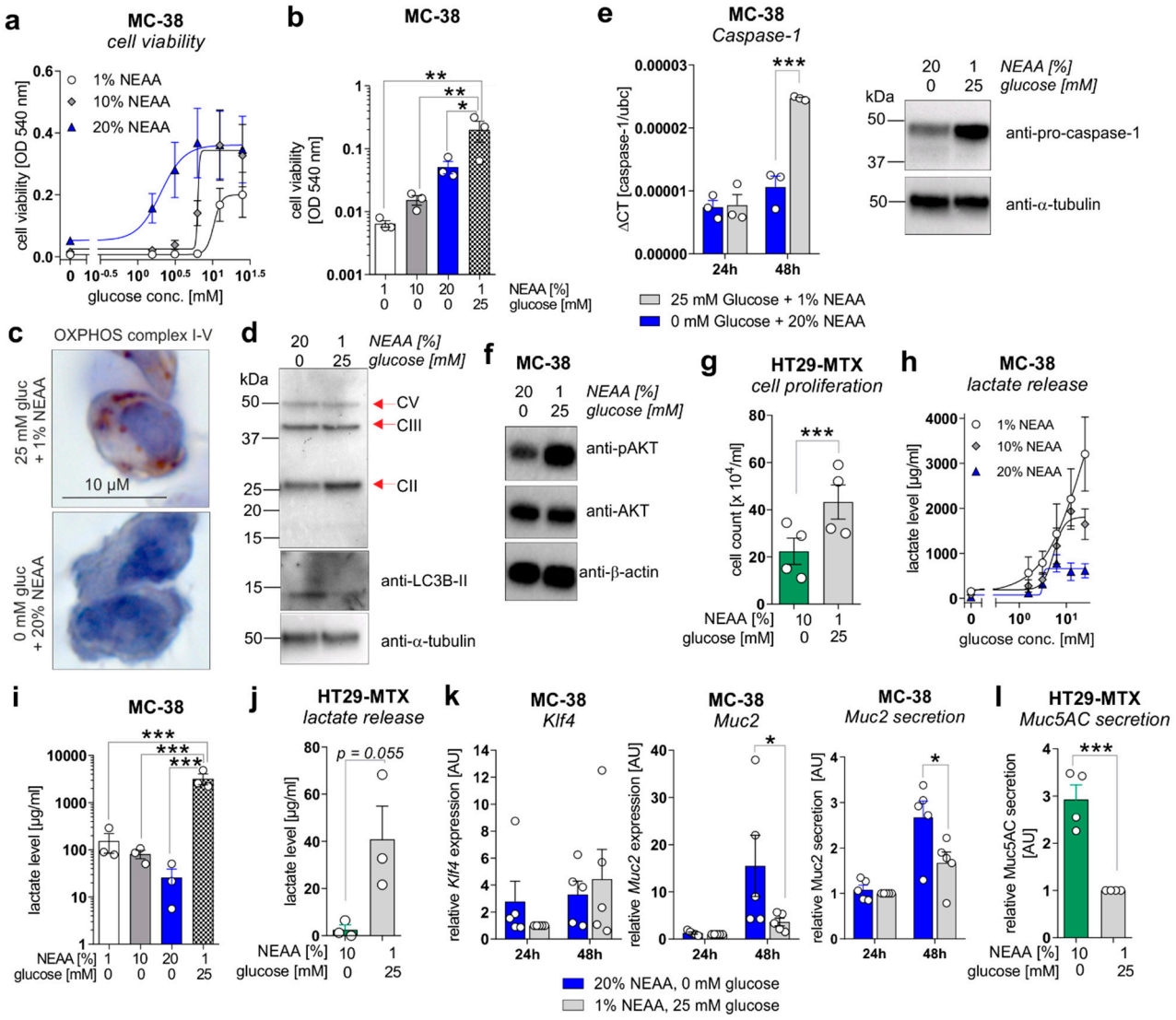

Figure 5. A metabolic shift from aerobic glycolysis towards amino acid metabolism inhibits proliferation but enhances goblet cell differentiation of CRC cell lines in vitro. (**a**,**b**) MC-38 cells were incubated in culture media containing increasing concentrations of D-glucose (0–25 mM) in the presence of 1%, 10%, or 20% NEAA. After 72 h, cell viability was determined by neutral red cytotoxicity assay. (**c**) Representative images of immunohistochemistry staining of paraffin-embedded MC-38 cells after 48 h cultivation under standard (25 mM glucose + 1% NEAA) or glucose-free (0 mM glucose + 20% NEAA) conditions, utilizing an antibody cocktail against OXPHOS complexes I–V. (**d**) MC-38 cells were incubated in standard culture medium (25 mM glucose, 1% NEAA) or in glucose-free plus 20% NEAA medium for 48 h. Expression of OXPHOS complexes II, III, and V or LC3B were analyzed by Western blot experiments. Alpha-Tubulin expression served as a loading control (representative images of $n = 3$ independent experiments). (**e**) MC-38 cells were incubated in a standard culture medium (25 mM glucose, 1% NEAA) or glucose-free plus 20% NEAA medium for 24 or 48 h. *Caspase-1* mRNA expression was quantified by qPCR experiments and related to *Ubc* mRNA expression (left panel; $n = 3$ independent experiments). Caspase-1 protein expression after 48 h of incubation was analyzed by Western blot experiments. Alpha-Tubulin expression served as a loading control (right panel; representative images of $n = 3$ independent experiments). (**f**) Protein levels of phosphorylated AKT and AKT were determined after 48 h of incubation of MC-38 cells under indicated culture conditions by Western blot experiments. β-actin expression served as a loading control. Representative images of $n = 3$ independent experiments. (**g**) HT29-MTX cells were incubated for 72 h under indicated culture conditions and cell count was determined. Mean ± SEM of four independent experiments is presented. (**h**,**i**) MC-38 cells were incubated under indicated culture conditions. After 72 h, L-lactate levels were quantified in cell culture supernatants. (**j**) L-lactate release by HT29-MTX cells after 72 h of incubation under indicated culture conditions. L-lactate concentrations were related to the respective cell count presented in (**g**). Mean ± SEM of three independent experiments is presented. (**k**) MC-38 cells were incubated in standard

culture medium (25 mM glucose, 1% NEAA) or in glucose-free plus 20% NEAA medium for 24 or 48 h. *Klf4*, *Muc2*, or *Ubc* mRNA expression was quantified by qPCR experiments (n = 3 independent experiments). ΔCT values were calculated by normalization of *Klf4* or *Muc2* to *Ubc* and related to values received from standard culture conditions at 24 h. Muc2 secretion was analyzed after 72 h of incubation in cell culture supernatants from respective cells by ELISA experiments. Data are related to cell viability determined by neutral-red cytotoxicity assay and presented as mean ± SEM. (**l**) Muc5AC release by HT29-MTX cells was measured after 72 h of incubation and related to respective cell counts. Values were normalized to Muc5AC secretion observed for standard culture conditions. * $p \leq 0.05$, ** $p \leq 0.01$. *** $p \leq 0.001$. AU = arbitrary units.

2.5. A Metabolic Switch from Glucose to Amino Acid Metabolism as Well as Anti-EGFR Ab Treatment Decreases PD-L1 Expression in CRC Cells and Colonic CD4$^+$ T-Cell Count

Metabolic active tumors create a tumor environment characterized by a high tumoral aerobic glycolysis activity driven lactate release that has been demonstrated to inhibit the anti-tumor immune responses of surrounding T cells and macrophages [17]. Hence, we analyzed the mRNA expression of leukocyte markers in colonic biopsy samples of analyzed mice (Figure 6a). While no differences in the expression of the pan-leukocyte marker *Cd45* were detected, the T cell specific *Cd4* marker, but not *Cd3e* or *Cd8a*, was significantly down-regulated in GFHPD vs. CD-fed mice treated with a ctrl. Ab. Furthermore, anti-EGFR Ab therapy did not alter *Cd3e* or *Cd4* expression in CD-fed mice but did significantly up-regulate both transcripts in GFHPD-fed mice (Figure 6b,c). No differences in mRNA expression were detected for markers specific for natural killer (NK) cells (*Cd69*; Figure 6a), plasma cells (*Bcma*; Figure 6a), macrophages (*F4/80*; Figure 6a), or granulocytes (*Ly6g*; Figure 6a). Based on the strong inhibitory effect of GFHPD on CD4$^+$ T-cell infiltration into the colonic compartment in AOM/DSS mice, we further quantified colonic expression of the immune checkpoints *Pd-1* and *Ctla4*, as well as their respective ligands *Pd-l1* and *Cd80* or *Cd86* (Figure 6a). Here, *Pd-1*, *Ctla4*, *Cd80*, or *Cd86* mRNA expression was comparable between the analyzed groups, while a trend towards down-regulation without statistical significance of *Pd-l1* expression in GFHPD (mean ± SD, 0.00034 ± 0.00025) vs. CD (mean ± SD, 0.001 ± 0.00034) fed mice treated with a ctrl. Ab was observed. Of note, anti-EGFR Ab treatment under a CD displayed a significantly lower *Pd-l1* expression when compared to anti-EGFR Ab treatment under a GFHPD (Figure 6d).

To functionally validate results received from ex vivo experiments, PD-L1 mRNA, as well as protein expression, was determined in the murine colorectal carcinoma cells MC-38. As depicted in Figure 6e,f, incubation of MC-38 cells in glucose-free plus 20% NEAA culture conditions for 48 h significantly reduced PD-L1 mRNA and protein expression in comparison to 25 mM glucose plus 1% NEAA culture conditions (Figure 6e,f). Additionally, we incubated MC-38 cells in the presence of either an anti-EGFR-mIgG2a Ab or a ctrl. Ab under glucose-free plus 20% NEAA or 25 mM glucose plus 1% NEAA culture conditions for 48 h. Of note, anti-EGFR Ab treatment of MC-38 cells induced a significant down-regulation of *Pd-l1* exclusively under glucose-containing plus 1% NEAA culture conditions, while no alterations were detected under glucose-free and 20% NEAA culture conditions (Figure 6g).

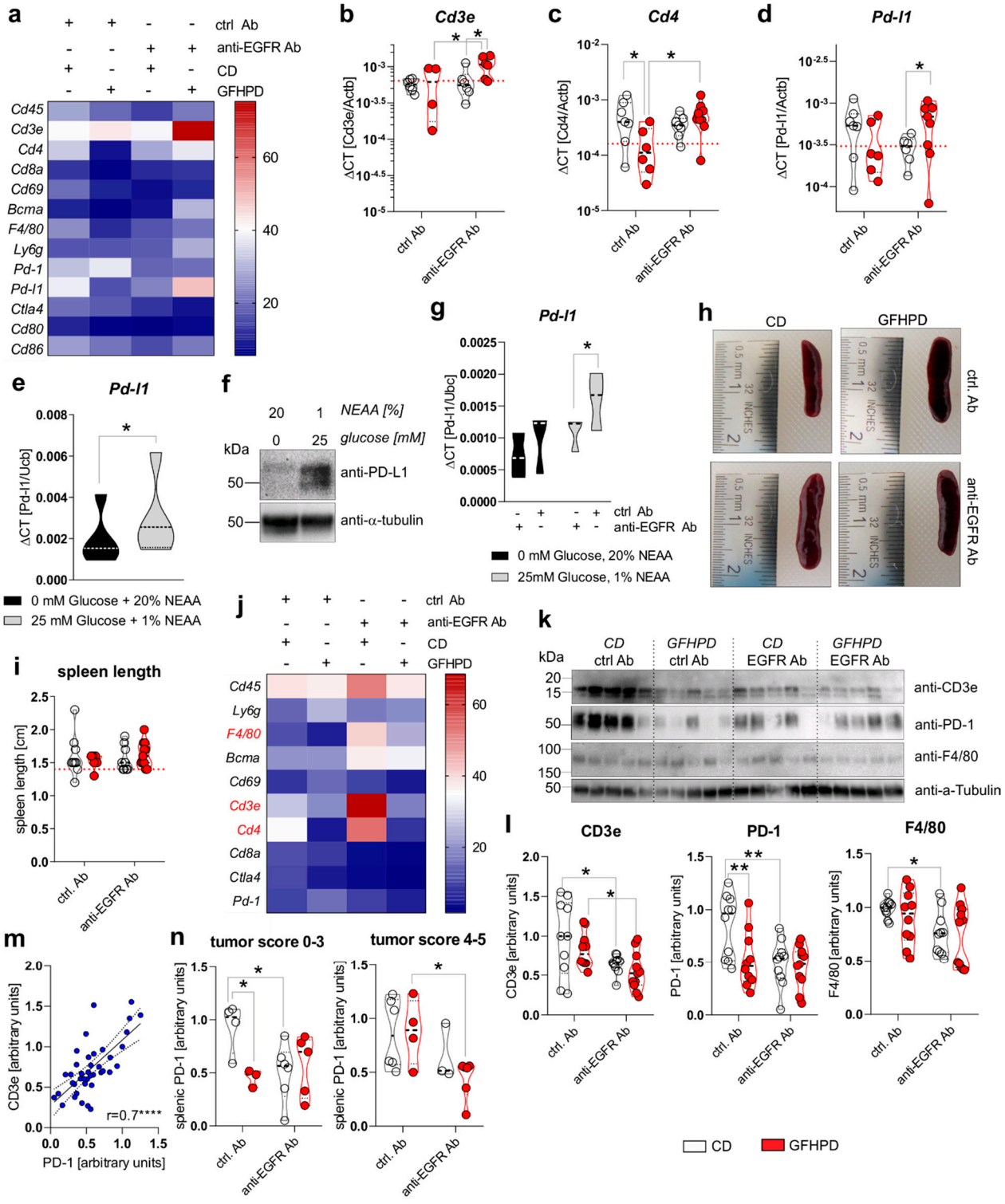

Figure 6. GFHPD and anti-EGFR Ab treatment reduce tumoral Pd-l1 expression and PD-1 expressing T cells. (**a**–**d**) QPCR analyses were performed to quantify mRNA expression level of *Cd45*, *Cd3e*, *Cd4*, *Cd8a*, *Cd69*, *Bcma*, *F4/80*, *Ly6g*, *Pd-1*, *Pd-l1*, *Ctla4*, *Cd80*, or *Cd86* in colonic tissues collected from indicated treatment groups of AOM/DSS mice. Results are based on ΔCT calculation including relation to β-actin mRNA expression. Heatmap was generated based on normalized values (%) per transcript. The mean value per group is presented. n = 6–7 ctrl. Ab and CD; n = 6–7 anti-EGFR Ab and CD; n = 4–6 ctrl. Ab and GFHPD; n = 6–9 anti-EGFR Ab and GFHPD. Red dotted horizontal lines represent respective median values of PBS-treated control mice at day 126. (**e**,**f**) MC-38 cells were incubated in standard culture medium (25 mM glucose, 1% NEAA) or glucose-free plus 20% NEAA medium for 48 h. (**e**) *Pd-l1* mRNA expression was quantified by qPCR experiments

and related to *Ubc* mRNA expression (n = 5 independent experiments), while (**f**) PD-L1 protein expression was analyzed by Western blot experiments. Alpha-Tubulin expression served as a loading control (representative images of n = 5 independent experiments). (**g**) MC-38 cells were incubated in standard culture medium (25 mM glucose, 1% NEAA) or in glucose-free plus 20% NEAA medium in the presence or absence of either the anti-EGFR Ab 7A7-mIgG2a or the irrelevant control Ab CD19-mIgG2a for 48 h. *Pd-l1* mRNA expression was quantified by qPCR experiments and related to *Ubc* mRNA expression (n = 3 independent experiments). (**h**) Representative images from spleens collected from AOM/DSS-treated mice at day 126. (**i**) Representative spleen lengths were measured for indicated treatment groups. n = 9 ctrl. Ab and CD; n = 9 anti-EGFR Ab and CD; n = 6 ctrl. Ab and GFHPD; n = 11 anti-EGFR Ab and GFHPD. Red dotted horizontal line represents median values of PBS-treated control mice at day 126. (**j**) QPCR analyses were performed to quantify mRNA expression levels of *Cd45*, *Ly6g*, *F4/80*, *Bcma*, *Cd69*, *Cd3e*, *Cd4*, *Cd8a*, *Ctla4*, and *Pd-1* in splenic tissues collected from indicated treatment groups of AOM/DSS mice. Results are based on $2^{-\Delta CT}$ calculation, including relation to β-actin mRNA expression. Heatmap was generated based on normalized values (%) per transcript. The mean value per group is presented. n = 10 ctrl. Ab and CD; n = 10 anti-EGFR Ab and CD; n = 10 ctrl. Ab and GFHPD; n = 11 anti-EGFR Ab and GFHPD. (**k**) Splenic CD3e, PD-1, and F4/80 protein expression levels were determined by Western blot experiments. Alpha-Tubulin expression served as a loading control. (**l**) Densitometric analyses were performed using ImageJ software. n = 10 ctrl. Ab and CD; n = 10 anti-EGFR Ab and CD; n = 10 ctrl. Ab and GFHPD; n = 11 anti-EGFR Ab and GFHPD. (**m**) Splenic PD-1 protein expression was related to splenic CD3e protein expression. (**n**) Splenic PD-1 protein expression is displayed in relation to colorectal tumor scores (smaller tumor 0–3; larger tumor 4–5). * $p \leq 0.05$, ** $p \leq 0.01$, **** $p \leq 0.0001$.

Together, these results demonstrate a significant up-regulation of PD-L1 in highly glycolytic CRC cells that can be prevented by GFHPD or anti-EGFR Ab application.

2.6. PD-1 Expression on Splenic T Cells Is Reduced under GFHP Diet or Anti-EGFR Ab Treatment in AOM/DSS-Treated Mice

Next, we investigated the effect of GFHPD consumption and anti-EGFR Ab treatment on the leukocyte marker expression in the splenic compartment that is crucially involved in anti-tumor immune responses [40]. Macroscopically, no differences were found between the analyzed groups regarding the size of the spleens (Figure 6h,i). Next, qPCR experiments were performed to identify potentially regulated subtypes of splenic leukocytes (Figure 6j). No differences in mRNA expression levels were detected for *Cd45*, *Ly6g*, *Bcma*, *Cd69*, *Cd8a*, *Ctla4*, and *Pd-1*. However, anti-EGFR Ab therapy in CD-fed mice was accompanied by the up-regulation of *F4/80*, *Cd3e*, and *Cd4*. In contrast, GFHPD consumption in ctrl. Ab-treated mice strongly reduced splenic *Cd3e* and *Cd4* expression, as already observed in the colonic compartment (Figure 6j). Next, Western blot experiments were performed with protein extracts from respective spleens collected from the analyzed mice (Figure 6k). In contrast to qPCR results, anti-EGFR Ab treatment was accompanied by significantly lower CD3ε and PD-1 protein expression levels under CD compared to the ctrl. Ab treatment group. Furthermore, PD-1 expression, but not CD3ε expression, was strongly reduced in ctrl. Ab-treated mice fed a GFHP diet when compared to those mice fed a CD. However, anti-EGFR Ab therapy of mice under a GFHPD displayed a significant down-regulation of splenic CD3ε expression in comparison to ctrl. Ab therapy. Notably, GFHPD consumption did not alter the expression of macrophage marker F4/80, while a significant reduction was detected under anti-EGFR Ab therapy in CD-fed mice when compared to ctrl. Ab therapy (Figure 6l). As splenic PD-1 expression highly correlated with splenic CD3e expression (Figure 6m), we subdivided PD-1 protein expression levels into mice harboring colorectal tumors with a score of 0–3 or 4–5. In mice harboring smaller colorectal tumors (score of 0–3), splenic PD-1 expression was significantly reduced under a GFHP diet (ctrl. Ab therapy) vs. CD or under anti-EGFR Ab therapy plus a CD. In contrast, mice harboring larger colorectal tumors (score 4–5) displayed significantly reduced splenic PD-1 expression exclusively after anti-EGFR Ab treatment under a GFHPD, while no differences were observed under a CD (Figure 6n).

In summary, GFHPD consumption efficiently reduced PD-1 and PDL-1 immune-checkpoint protein expression to a comparable extent as anti-EGFR Ab therapy, suggesting both therapeutic regimens to boost anti-tumor T-cell responses.

3. Discussion

In this study, we identified a glucose-free, high-protein diet (GFHPD) to prevent high glycolysis activity while boosting amino acid metabolism, thereby reducing CRC burden with similar efficacy as EGFR-directed antibody therapy in an experimental mouse model of colitis-driven CRC. Furthermore, therapeutic application of a GFHPD or anti-EGFR Ab to mice harboring established CRC tumors significantly reduced systemic glycolysis activity, thereby promoting intestinal goblet cell differentiation. In contrast to reduced colonic expression of OXPHOS complex IV, a GFHPD, but not anti-EGFR Ab therapy, significantly increased the colonic expression of mitochondrial markers such as p32 and TOM20, potentially resulting in a more quiescent glycolysis/OXPHOS balanced colonic metabolism that is highly present in differentiated tissues. Furthermore, we recently published p32 to be highly expressed in goblet cells and to play a crucial role in OXPHOS-driven colonic goblet cell differentiation in normal large intestines [37]. According to studies demonstrating mucus production to be strongly decreased in CRC [41–43], heterozygous expression of the most prominent single nucleotide polymorphism (SNP) in p32 *rs56014026* was characterized to maintain quiescent metabolism and goblet cell differentiation of CRC cells and to be expressed in low-grade colorectal carcinomas in patients [44]. Hence, GFHPD or anti-EGFR antibody therapy associated reduction in colonic OXPHOS activity but improved goblet cell differentiation points to metabolic reprogramming of colorectal carcinomas towards a low-energetic balanced metabolism, thereby preventing cell proliferation and CRC tumor progression. The concept of dietary carbohydrate reduction in tumor therapy constitutes an old concept that is gaining increased acceptance today [45]. One of the first studies directly demonstrating that the isoenergetic replacement of some carbohydrate portions by proteins reduces skin or mammary tumor formation in mice was published by Tannenbaum in 1945 [46]. These data were further validated by Ho et al., who further decreased dietary carbohydrate content to 8% combined with an isoenergetic replacement by increased protein fraction. In this study, murine squamous cell carcinoma cell line SCCVII or human colorectal carcinoma cell line HCT-116 xenografts displayed diminished tumor growth in male, but not female, mice fed a low-carbohydrate and high-protein diet [47].

Besides enhancement of CRC goblet cell differentiation, both therapeutic regimens, GFHPD or anti-EGFR antibody therapy, strongly dampened colonic PD-L1 and splenic T-cell specific PD-1 immune checkpoint expression, presumably promoting improved anti-tumor immune responses. In detail, ctrl. Ab therapy under GFHPD intervention compared to a CD did not alter colonic *Cd3e* or *Cd8a* expression, while *Cd4* and *Pd-l1* were down-regulated. Hence, one may hypothesize that GFHPD consumption mainly reduces expansion/infiltration of colonic $CD4^+$ T cells but not of $CD8^+$ T cells. This is in line with findings demonstrating high tumoral $CD8^+$ cell density, but not $CD3^+$ cell density, to be associated with a lower risk of recurrence in CRC patients [48,49]. $CD8^+$ T cells, especially $CD8^+$ cytotoxic T cells, display one of the major immune cell types for tumor cell destruction that is a high-energy-demanding immune cell, mainly performing high glycolysis and OXPHOS activities, as well as glutaminolysis [50]. In the splenic compartment, we observed a strong down-regulation of CD3ε and PD-1 expression under ctrl. Ab therapy plus a GFHPD, as well as under anti-EGFR antibody therapy (CD and GFHPD). Due to data revealing PD-1 to be prominently expressed on $CD4^+$ tumor-infiltrating lymphocytes (TILs) and to a lesser extent on $CD8^+$ TILs [51], we could speculate that $CD4^+$ T cells highly depend on glycolysis, while $CD8^+$ T cells are able to better compensate low glycemic diets. Furthermore, due to the strong inhibition of anti-tumor T cell responses via binding of tumor cell-expressed PD-L1 to T cell expressed PD-1 [51,52], decreased PD-1 expression on circulating splenic T cells in combination with decreased colonic PD-L1 expression in the present study may result in improved anti-tumor T cell responses in CRC mice treated either with a GFHPD or with an anti-EGFR antibody. Recent publications also unraveled EGFR to be expressed on $CD4^+$ T cells and that the EGFR-specific tyrosine kinase inhibitor erlotinib inhibits $CD4^+$ T cell proliferation in vitro, while a $CD4^+$ T cell specific deletion of *Egfr* in mice was also accompanied by a loss of T cell activation and proliferation

in vivo [53]. Hence, anti-EGFR antibody therapy applied to CRC mice in the present study may reduce the splenic $CD4^+$ T cell load via EGFR blockade on $CD4^+$ T cells, as well as by induction of Fc-mediated effector cell cytotoxicity against $CD4^+$ T cells [54].

One major advantage of a glucose-free, high protein nutritional intervention as a single therapeutic regimen in CRC patients may be the independence of tumor mutational profiles or EGFR cell surface expression levels. However, in contrast to nutritional intervention, the efficacy of anti-EGFR antibody therapy strongly depends on the tumoral EGFR expression level [54,55], as well as on the absence of activating mutations of the RAS protein family members [56–58]. Hence, one may hypothesize that the combination of GFHPD and anti-EGFR Ab therapy may be beneficial in low EGFR expressing CRC tumors, while the single GFHPD application may be efficacious in the therapy of RAS mutated CRC tumors.

Notably, in the present study, we applied a glucose-free, casein-enriched diet to mice with pre-existing CRC tumors to achieve a reduction of glycolysis and the pentose-phosphate pathway, thereby restraining tumor metabolism. Unexpectedly, consumption of this glucose-free, high-protein diet for more than two months was not accompanied by weight loss, a reduction of blood glucose level, or altered behavior of mice. These data highlight the hypothesis that mice can compensate for nutritional glucose deprivation and use a protein source to maintain blood glucose levels. However, diets high in protein fraction are known to enhance renal function and may affect kidney health. Indeed, we observed a significant increase in water consumption by mice fed a GFHP diet but without any morphological impact on the analyzed kidneys. Previously, consumption of a protein-rich diet was accompanied by increased renal blood flow and elevated intraglomerular pressure, resulting in enhanced glomerular filtration rates [59–61]. In the present study, casein, a protein derived from cow's milk, served as the primary energy source. One disadvantage of this chosen GFHPD may be the transfer to nutritional intervention studies in humans. Interestingly, besides high fiber or low alcohol intake, diets rich in dairy proteins have been associated with a decreased risk of CRC development in humans [4,62].

To conclude, consumption of a glucose-free, high protein diet (GFHPD), comparable to EGFR-directed antibody-based therapy, efficaciously dampens colorectal tumor burden but does not have additive effects in combination with anti-EGFR therapy. In addition, a GFHPD boosts amino acid metabolism, resulting in improved tumor differentiation and anti-tumor immune responses.

4. Materials and Methods

4.1. Animal Experiments

All animal experiments were approved by the ethics committee, Schleswig-Holstein, Germany (V 242–27664/2018 (64–5/17)) and were performed in two independent experimental rounds. Mice were maintained at the University of Lübeck under specific pathogen-free conditions at a regular 12 h light–dark cycle with access to food and water *ad libitum*.

Procedures involving animals and their care were conducted in accordance with national and international laws and regulations. Glucose-free high protein diet (GFHPD) and isoenergetic control diet (CD) were purchased from Ssniff (Soest, Germany). Compositions of corresponding diets are specified in Table 1. To perform an isoenergetic exchange of carbohydrates by proteins, the fat content was increased from 14 to 32% of energy intake. Female C57BL/6 mice (n = 107) were ordered at the age of 7–8 weeks from Charles River (Wilmington, MA, USA) and were left to acclimatize on a standard chow diet (Altromin #1324, Lage, Germany). At the age of 10 weeks (day 0), one group (n = 88) initially received 10 mg/kg/BW AOM via intraperitoneal (*i.p.*) injection, while the second control group (n = 19) received *i.p.* injection of 1× PBS. Experimental chronic colitis was induced in mice on day 7 by administration of 2% (w/v) dextran sodium sulfate (DSS; Batch DB001-27, molecular mass 40 kDa; TdB Consultancy, Uppsala, Sweden) dissolved in the drinking water for 7 d, followed by normal drinking water ad libitum. A second *i.p.* injection of 5 mg/kg/BW AOM or 1× PBS was performed on day 21. On day 42, mice either received

a second administration of 1% (*w*/*v*) DSS via the drinking water or were left untreated until day 45. On day 70, indicator mice (n = 9 AOM/DSS-treated; n = 8 PBS-treated) mice were euthanized, and high-resolution mouse video endoscopy was applied (Hopkins Optik 64019BA; Aida Vet; Karl Storz, Tuttlingen, Germany) to obtain the murine endoscopic index of colitis severity (MEICS) [33]. The remaining mice were randomly distributed on day 70 into GFHPD (n = 40) and isoenergetic CD (n = 39) receiving groups until day 126. Mice were kept on the corresponding diet on an average of 56 days before sampling. In AOM/DSS-treated mice (d0–70), the two dietary intervention groups were subdivided into following groups of weekly *i.p.* applications: 1× PBS (n = 9 CD; n = 9 GFHPD), anti-EGFR Ab (7A7-mIgG2a [25,27,28]; initial dose of 879 µg/kg/BW at day 70, weekly dose of 563 µg/kg/BW; n = 15 CD; n = 16 GFHPD) or an irrelevant ctrl. antibody (CD19-mIgG2a; initial dose of 879 µg/kg/BW at day 70, weekly dose of 549 µg/kg/BW; n = 15 CD; n = 15 GFHPD). PBS-treated control mice (d0–70) were fed either CD (n = 5) or GFHPD (n = 6) between day 70 and 126. Food and water consumption and body weight were monitored weekly. The modified disease activity index (DAI) was assessed routinely as a combined score of weight loss (0 = none, 1 = 1–5%, 2 = 5–10%, 3 = 10–15%, 4 = 15–20%), stool consistency (0 = solid, 2 = soft, 3 = diarrhea), and rectal bleeding, determined by a fecal occult blood test (0 = no blood, 2 = positive, 4 = gross blood). Animals that lost more than 20% of their initial weight were euthanized. At the end of the experiment, colonoscopy was performed in sedated animals utilizing high-resolution mouse video endoscopy (Hopkins Optik 64019BA, Aida Vet), and tumor scores were determined according to [33]. Afterwards, mice were sacrificed, and clinical parameters were assessed.

4.2. Histology and Microscopy Analyses

Immunohistochemical staining in paraformaldehyde (PFA)-fixed and paraffin-embedded tissue biopsies or MC-38 cells was performed according to standard protocols. After deparaffinization, rehydration, antigen retrieval, and endogenous peroxidase blockage, tissue slides were probed with a specific primary antibody against murine EGFR or an isotype control antibody, followed by respective HRP-conjugated secondary antibody. Tissue slides were incubated with DAB-substrate (Dako, Jena, Germany) and counterstained with Mayer's hemalum solution. Histochemical staining was performed by staining tissue slides with hematoxylin-eosin (HE), periodic acid–Schiff (PAS), or Alcian blue solutions. Images were obtained and analyzed on an Axio Scope.A1 microscope (Zeiss, Oberkochen, Germany) utilizing the ZEN imaging software (Zeiss).

4.3. Metabolic Analyses in Serum Samples

Murine whole blood samples were collected, placed on ice for 30 min, and centrifuged at 500× *g* and 4 °C for 5 min. Serum samples were transferred to new vials and stored at −80 °C. Serum levels of L-lactate (Megazyme, Wicklow, Ireland), glucose (Analyticon® Biotechnologies AG, Lichtenfels, Germany), insulin (Thermo Fisher Scientific Inc., Waltham, MA, USA), C-peptide (RayBiotech Life, Inc., Peachtree Corners, GA, USA), branched-chain amino acids (BCAA; Sigma-Aldrich, St. Louis, MO, USA), or L-alanine (AAT Bioquest, Inc., Sunnyvale, CA, USA) were measured in diluted serum samples according to manufacturer's instructions. Optical densities were measured on a SpectraMax iD3 microplate reader (Molecular Devices, San José, CA, USA).

4.4. Cell Culture

The murine colorectal carcinoma cell line MC-38, derived from C57BL/6 mice (Kerafast Inc., Boston, MA, USA), and the human colorectal carcinoma cell line HT29-MTX-E12 (Sigma-Aldrich, St. Louis, MO, USA) were kept in DMEM medium supplemented with 1% non-essential amino acids (NEAA). All cell culture media were supplemented with 10% (*v*/*v*) heat-inactivated FCS, 100 U/mL penicillin, and 100 mg/mL streptomycin. Cells were incubated at 37 °C and 5% CO_2 in a humidified incubator. Cells were cultivated up to a maximum of 20 passages and confirmed to be negative for mycoplasma contamina-

tion every three months and when freshly thawed. For D-glucose and NEAA titration experiments, cells were seeded in glucose-free DMEM medium supplemented with 10% FCS, 100 U/mL penicillin, and 100 mg/mL streptomycin, and D-glucose and/or NEAA solutions were added at indicated concentrations.

4.5. RNA Extraction, cDNA Synthesis and Quantitative PCR

RNA was extracted with the innuPREP RNA mini kit (Analytik Jena AG, Jena, Germany) and transcribed to cDNA (RevertAid H Minus reverse transcriptase; Thermo Fisher Scientific, Waltham, MA, USA) using the T Gradient thermocycler (Whatman Biometra, Göttingen, Germany). Quantitative PCR (qPCR) was performed on the StepOne real-time system (ThermoFisher Scientific, Waltham, MA, USA), applying Perfecta SYBR Green Supermix (ThermoFisher Scientific, Waltham, MA, USA). Following cycling conditions were applied: initial denaturation at 95 °C for 5 min; 40 cycles of denaturation at 95 °C for 45 s, annealing at appropriate temperature (55 °C) for 30 s and elongation for 30 s at 72 °C. Melting curve profiles were produced, and data were analyzed following the $2^{-\Delta Ct}$ algorithm by normalization to *β-actin* or *Ubc*. Primer sequences are listed in Table 2.

Table 2. Information on applied primer pairs.

Target Transcripts	Forward Primer (5′–3′)	Reverse Primer (5′–3′)
Atoh1	GTGGGGTTGTAGTGGACGAG	GTTGCTCTCCGACATTGGG
Actb	GATGCTCCCCGGGCTGTATT	GGGGTACTTCAGGGTCAGGA
Klf4	GATTAAGCAAGAGGCGGT	GGTAAGGTTTCTCGCCTGTG
Lgr5	CGGCAACAGTGTGGACGACCT	GCGAGCACTGCACCGAGTGA
Muc2	GCTGACGAGTGGTTGGTGAATG	GATGAGGTGGCAGACAGGAGAC
Spdef1	GGAGAAGGCAGCATCAGGA	CCAGGGTCTGCTGTGATGT
Hes1	CAAACCAAAGACGGCCTCT	GTCACCTCGTTCATGCACTC
Egfr	ATGTGATCCAAGCTGTCCCA	CTGATAGGTGGTGGGGTTGT
Caspase-1	CTTCAATCAGCTCCATCAGC	CACGGCATGCCTGAATAATG
C3	GACGCCACTATGTCCATC	GAAGGTCAGGCAGTCTTC
PD-L1	GCTACGGGCGTTTACTATCAC	CTGAATCACTTGCTCATCTTCC
Cd80	CAAGTGTCTTCAGATGTTGATGAAC	GAACGACACAGCTGTATGTGC
Cd86	CTCAGATGCTGTTTCCGTGG	GTTCCTGTCAAAGCTCGTGC
Cd3e	AGTTGACGTGCCCTCTAGAC	ATCAGCAAGCCCAGAGTGAT
Cd4	TTTGCAGAGGAAAACGGGTG	CTGCTTCAGGGTCAGTCTCA
Cd45	TCATGGTCACACGATGTGAAGA	AGCCCGAGTGCCTTCCT
Cd8a	GAAGTGTTGGGGTCCGTTTC	TCACCGAGTTGCTGATGACT
Cd69	CAGAAGGACCATGGCACCA	CGTCAAGTTGAACCAGCTG
Bcma	GGTGCTCTGGATCTTCTTGG	CCGTAGTCACCCGTTTTTGT
F4/80	CTGTAACCGGATGGCAAACT	CATCACTGCCTCCACTAGCA
Ly6g	GATGGATTTTGCGTTGCTCTG	GGACTGAAACCAGGCTGAAC
Pd-1	GTGGTAACAGAGAGAATCCTGGA	ACTAGGGACAGGTGCTGCTG
Ctla-4	GAAGCCATACAGGTGACCCA	TGAATGTCGTGGCACAGACC

4.6. Sodium Dodecyl Sulfate Polyacrylamide Gel Electrophoresis (SDS-PAGE) and Immunoblotting

SDS-PAGE and immunoblotting were performed according to standard protocols. In short, whole-protein extracts from homogenized tissue samples or cells were prepared by cell lysis in denaturing lysis buffer containing 1% (*w*/*v*) SDS, 10 mM Tris (pH 7.4), phosphatase II, phosphatase III, and protease inhibitor (Sigma-Aldrich, St. Louis, MO, USA). For extraction of proteins from fecal samples, 50 mg of feces was resuspended in 1 mL 0.5% (*v*/*v*) Tween, 0.05% (*w*/*v*) sodium azide in PBS, and centrifuged at 12,000× *g* for 15 min at 4 °C. Supernatant was taken off, protease inhibitor cocktail (Sigma-Aldrich, St. Louis, MO, USA) was added, samples were centrifuged as stated above, and supernatant was taken for further analysis. Protein extracts were separated by denaturing SDS-PAGE (Bio-Rad Laboratories, Hercules, CA, USA) under reducing conditions and transferred onto polyvinylidene difluoride membranes. After blocking, membranes were probed with

specific primary antibodies followed by respective HRP-conjugated secondary antibodies. To determine similar transfer and equal loading, membranes were stripped and reprobed with an antibody against an appropriate housekeeper. Proteins of interest were visualized on a ChemiDocTM XRS$^+$ Imaging System (Bio-Rad Laboratories, Hercules, CA, USA). In the case of Western blot experiments against fecal C3, both Western blots were performed in parallel at the same time (gel loading and running, blotting in the same chamber) utilizing 10 µg of protein extracts from each sample. Furthermore, visualization was also performed at the same time by putting both gels into the ChemiDocTM XRS$^+$ Imaging System (Bio-Rad Laboratories, Hercules, CA, USA) and taking an image at 164.5 s of exposure time. Applied antibodies are listed in Table 3. Densitometric analyses were performed using the software ImageJ version 1.53e (National Institutes of Health, Bethesda, MD, USA). The full blots can be found in Figure S1.

Table 3. Details of applied primary and secondary antibodies.

Primary Antibodies	Species	Company	Working Concentration
Anti-AMPKα (#2532)	rabbit	Cell Signaling, Danvers, MA, USA	1:1000 [a]
Anti-β-Actin (#4967)	rabbit	Cell Signaling, Danvers, MA, USA	1:1000 [a]
Anti-α-TUBULIN (#2125)	rabbit	Cell Signaling, Danvers, MA, USA	1:1000 [a]
Anti-Caspase-1 (ab179515)	rabbit	Abcam, Cambridge, UK	1 µg/mL
Anti-MUC2 (C3) (GTX100664)	rabbit	Genetex, Alton Pkwy Irvine, CA, USA	1 µg/mL
Anti-Muc5AC (clone 45M1) (GTX11335)	mouse	Bioss, Woburn, MA, USA	1 µg/mL
Anti-pAMPKα (Thr172, #2535)	rabbit	Cell Signaling, Danvers, MA, USA	1:1000 [a]
Anti-pAkt (Ser473) (D9E) (#4060)	rabbit	Cell Signaling, Danvers, MA, USA	1:1000 [a]
Anti-Akt (#9272)	rabbit	Cell Signaling, Danvers, MA, USA	1:1000 [a]
Anti-EGFR (EP38Y) (ab52894)	rabbit	Abcam, Cambridge, UK	1:1000 [a]
Anti-PD-L1 (B7-H1) (MAB90781)	rabbit	R&D Systems, Minneapolis, MN, USA	1 µg/mL
Anti-p32 (clone EPR8871) (ab131284)	rabbit	Abcam, Cambridge, UK	0.4 µg/mL
Anti-Tom20 (D8T4N) (#42406)	rabbit	Cell Signaling, Danvers, MA, USA	1:1000 [a]
Anti-LDHA/C (C28H7) (#3558)	rabbit	Cell Signaling, Danvers, MA, USA	1:1000 [a]
Anti-CD3ε (ab5690)	rabbit	Abcam, Cambridge, UK	1 µg/mL
Anti-F4/80 (MA5-16363)	rabbit	Thermo Fisher Scientific Inc., Waltham, MA, USA	0.2 µg/mL
Anti-mEGFR (7A7-mIgG2a) (Ab00134-23.0)	mouse	Absolute Antibody NA, Boston, MA, USA	
CD19-mIgG2a (FMC63) (Ab00613-2.0)	mouse	Absolute Antibody NA, Boston, MA, USA	
Anti-OXPHOS complexes I-V	mouse	Thermo Fisher Scientific Inc., Waltham, MA, USA	6 µ/mL
Anti-LC3B (#2775)	rabbit	Cell Signaling, Danvers, MA, USA	1:1000 [a]
Secondary Antibodies		**Company**	**Working Concentration**
Anti-mouse IgG HRP		Cell Signaling, Danvers, MA, USA	1:1000 (ELISA) [a]
Anti-rabbit IgG HRP		Cell Signaling, Danvers, MA, USA	1:2000 (ELISA) [a]; 1:4000 (WB) [a]

[a] If stock concentration was not provided by the manufacturer, dilution from stock solution was listed.

4.7. Neutral Red Cytotoxicity Assay

The neutral red cytotoxicity assay was performed to determine the viable cell mass of MC-38 cells. A number of 5×10^3 cells per well were seeded into a 96-well microtiter plate and incubated at 37 °C and 5% CO_2 for 72 h. After incubation, cells were stained using a neutral red dye (Sigma-Aldrich, St. Louis, MO, USA), diluted 1:100 in DMEM medium for 2 h, and washed and destained with a solution consisting of 50% pure ethanol, 49% bidistilled water, and 1% pure acetic acid to release the incorporated dye into the supernatant. To analyze the neutral red dye uptake, absorbance was measured at 540 nm against a background absorbance of 690 nm on a SpectraMax iD3 microplate reader (Molecular Devices, San José, CA, USA).

4.8. Muc2 and Muc5AC ELISA

For detection of Muc2 or Muc5AC secretion by MC-38 or HT29-MTX cells, respectively, supernatants were centrifuged at 12,000× *g* and 4 °C for 15 min before coating into highly absorptive 96-well microtiter plates at 4 °C overnight. After blocking, Muc2 or Muc5AC was detected using primary antibodies specific for Muc2 or Muc5AC in combination with respective HRP-conjugated secondary antibodies listed in Table 3. Optical density was measured at 450 nm against a reference wavelength of 540 nm on a SpectraMax iD3 microplate reader (Molecular Devices, San José, CA, USA).

4.9. Statistics

Statistical analysis was performed using the GraphPad Prism version 8.0.1 (San Diego, CA, USA). Outliers were identified by ROUT test. The F test was used to compare variances, and the D'Agostino–Pearson test was applied to test for normal distribution. Statistical differences between two groups were analyzed by unpaired t-test or paired t-test (normally distributed data), unpaired t-test with Welch's correction (significant different variances), or Mann–Whitney U test (not-normally distributed data). For comparison of more than two groups and two variables, two-way analysis of variances (ANOVA) with uncorrected Fisher's least significant difference test was employed. Correlation analysis was performed by obtaining the Pearson's correlation coefficient. *p*-values were calculated, and null hypotheses were rejected when $p \leq 0.05$.

5. Conclusions

Together, we here provided a novel therapeutic strategy to reduce CRC burden by applying a glucose-free, high-protein containing diet as a therapeutic regimen that systematically shifts glucose metabolism to amino acid metabolism, thereby restraining tumoral metabolism to prevent a high-energetic and fast proliferating state. Furthermore, a single application of a GFHPD to CRC-bearing mice displayed comparable therapeutic efficacy to an EGFR-directed antibody-based therapy, while the combination of both strategies did not result in an additive effect.

Supplementary Materials: The following are available online at https://www.mdpi.com/article/10.3390/cancers13225817/s1, Figure S1: Full western blots.

Author Contributions: S.D. designed the concept of the study and supervised it. K.S., A.-K.B., A.S., M.H., H.S., J.P., J.B., M.R., B.F., R.P., and S.D. performed the experiments and acquired the data. K.S., C.S., and S.D. analyzed and interpreted the data. S.D., A.R., M.R., and A.S. drafted the article. K.S., D.C., J.U.M., C.S., and S.D. critically revised the article. All authors have read and agreed to the published version of the manuscript.

Funding: This work was supported by the German Research Foundation (Research grant DE 1874/1-2 to SD) and an intramural grant from the University of Lübeck (H03-2020 to SD). C.S. is a Fresenius Kabi endowed professor for Nutritional Medicine.

Institutional Review Board Statement: All animal experiments were approved by the ethics committee, Schleswig-Holstein, Germany (V 242–27664/2018 (64-5/17)) and were performed in two independent experimental rounds. Procedures involving animals and their care were conducted in accordance with national and international laws and regulations.

Informed Consent Statement: Not applicable.

Data Availability Statement: The data presented in this study are available in this article (and Supplementary Material).

Acknowledgments: The authors gratefully thank Nieves Baenas and Katharina Schlumm for helping with organ sampling during animal studies.

Conflicts of Interest: The authors declare no conflict of interest.

References

1. Vuik, F.E.; Nieuwenburg, S.A.; Bardou, M.; Lansdorp-Vogelaar, I.; Dinis-Ribeiro, M.; Bento, M.J.; Zadnik, V.; Pellise, M.; Esteban, L.; Kaminski, M.F.; et al. Increasing incidence of colorectal cancer in young adults in Europe over the last 25 years. *Gut* **2019**, *68*, 1820–1826. [CrossRef] [PubMed]
2. Fatemi, S.R.; Pourhoseingholi, M.A.; Asadi, F.; Vahedi, M.; Pasha, S.; Alizadeh, L.; Zali, M.R. Recurrence and Five-Year Survival in Colorectal Cancer Patients After Surgery. *Iran. J. Cancer Prev.* **2015**, *8*, e3439. [CrossRef] [PubMed]
3. Francescangeli, F.; De Angelis, M.L.; Zeuner, A. Dietary Factors in the Control of Gut Homeostasis, Intestinal Stem Cells, and Colorectal Cancer. *Nutrients* **2019**, *11*, 2936. [CrossRef]
4. GBD 2017 Colorectal Cancer Collaborators. The global, regional, and national burden of colorectal cancer and its attributable risk factors in 195 countries and territories, 1990–2017: A systematic analysis for the Global Burden of Disease Study 2017. *Lancet Gastroenterol. Hepatol.* **2019**, *4*, 913–933. [CrossRef]
5. Terzic, J.; Grivennikov, S.; Karin, E.; Karin, M. Inflammation and colon cancer. *Gastroenterology* **2010**, *138*, 2101–2114.e5. [CrossRef]
6. Cooks, T.; Pateras, I.S.; Tarcic, O.; Solomon, H.; Schetter, A.J.; Wilder, S.; Lozano, G.; Pikarsky, E.; Forshew, T.; Rosenfeld, N.; et al. Mutant p53 prolongs NF-kappaB activation and promotes chronic inflammation and inflammation-associated colorectal cancer. *Cancer Cell* **2013**, *23*, 634–646. [CrossRef] [PubMed]
7. Liang, J.; Nagahashi, M.; Kim, E.Y.; Harikumar, K.B.; Yamada, A.; Huang, W.C.; Hait, N.C.; Allegood, J.C.; Price, M.M.; Avni, D.; et al. Sphingosine-1-phosphate links persistent STAT3 activation, chronic intestinal inflammation, and development of colitis-associated cancer. *Cancer Cell* **2013**, *23*, 107–120. [CrossRef]
8. Mendelsohn, J. Targeting the epidermal growth factor receptor for cancer therapy. *J. Clin. Oncol.* **2002**, *20*, 1S–13S.
9. Hanahan, D.; Weinberg, R.A. Hallmarks of cancer: The next generation. *Cell* **2011**, *144*, 646–674. [CrossRef]
10. Ciardiello, F.; Tortora, G. EGFR antagonists in cancer treatment. *N. Engl. J. Med.* **2008**, *358*, 1160–1174. [CrossRef]
11. Reichert, J.M.; Dhimolea, E. The future of antibodies as cancer drugs. *Drug Discov. Today* **2012**, *17*, 954–963. [CrossRef]
12. Baselga, J.; Mendelsohn, J. Epidermal growth factor receptor targeting in cancer. *Sem. Oncol.* **2006**, *33*, 369–385. [CrossRef]
13. Sinha, A.; Nightingale, J.; West, K.P.; Berlanga-Acosta, J.; Playford, R.J. Epidermal growth factor enemas with oral mesalamine for mild-to-moderate left-sided ulcerative colitis or proctitis. *N. Engl. J. Med.* **2003**, *349*, 350–357. [CrossRef]
14. Dubé, P.; Polk, D. P-186 YI Opposing Roles for EGFR in Colitis-Associated Cancer: The Presence of Active Inflammation Determines a Protective Versus Tumorigenic Role for EGFR. *Inflamm. Bowel Dis.* **2012**, *18*, S89–S90. [CrossRef]
15. Dube, P.E.; Yan, F.; Punit, S.; Girish, N.; McElroy, S.J.; Washington, M.K.; Polk, D.B. Epidermal growth factor receptor inhibits colitis-associated cancer in mice. *J. Clin. Investig.* **2012**, *122*, 2780–2792. [CrossRef] [PubMed]
16. Warburg, O. On the origin of cancer cells. *Science* **1956**, *123*, 309–314. [CrossRef] [PubMed]
17. Vander Heiden, M.G.; Cantley, L.C.; Thompson, C.B. Understanding the Warburg effect: The metabolic requirements of cell proliferation. *Science* **2009**, *324*, 1029–1033. [CrossRef] [PubMed]
18. Reitzer, L.J.; Wice, B.M.; Kennell, D. Evidence that glutamine, not sugar, is the major energy source for cultured HeLa cells. *J. Biol. Chem.* **1979**, *254*, 2669–2676. [CrossRef]
19. Rossignol, R.; Gilkerson, R.; Aggeler, R.; Yamagata, K.; Remington, S.J.; Capaldi, R.A. Energy substrate modulates mitochondrial structure and oxidative capacity in cancer cells. *Cancer Res.* **2004**, *64*, 985–993. [CrossRef]
20. Lunt, S.Y.; Vander Heiden, M.G. Aerobic glycolysis: Meeting the metabolic requirements of cell proliferation. *Annu. Rev. Cell Dev. Biol.* **2011**, *27*, 441–464. [CrossRef]
21. Dang, C.V. Links between metabolism and cancer. *Genes Dev.* **2012**, *26*, 877–890. [CrossRef]
22. Yang, P.; Li, Z.; Zhang, L.; Li, H.; Li, Z. Analysis of metabonomic profiling alterations in a mouse model of colitis-associated cancer and 2-deoxy-d-glucose treatment. *RSC Adv.* **2016**, *6*, 58862–58870. [CrossRef]
23. Lim, S.O.; Li, C.W.; Xia, W.; Lee, H.H.; Chang, S.S.; Shen, J.; Hsu, J.L.; Raftery, D.; Djukovic, D.; Gu, H.; et al. EGFR Signaling Enhances Aerobic Glycolysis in Triple-Negative Breast Cancer Cells to Promote Tumor Growth and Immune Escape. *Cancer Res.* **2016**, *76*, 1284–1296. [CrossRef] [PubMed]
24. Garrido, G.; Sanchez, B.; Rodriguez, H.M.; Lorenzano, P.; Alonso, D.; Fernandez, L.E. 7A7 MAb: A new tool for the pre-clinical evaluation of EGFR-based therapies. *Hybrid. Hybridomics* **2004**, *23*, 168–175. [CrossRef] [PubMed]
25. Van Buren, G., 2nd; Yang, A.D.; Dallas, N.A.; Gray, M.J.; Lim, S.J.; Xia, L.; Fan, F.; Somcio, R.; Wu, Y.; Hicklin, D.J.; et al. Effect of molecular therapeutics on liver regeneration in a murine model. *J. Clin. Oncol.* **2008**, *26*, 1836–1842. [CrossRef]
26. Garrido, G.; Lorenzano, P.; Sanchez, B.; Beausoleil, I.; Alonso, D.F.; Perez, R.; Fernandez, L.E. T cells are crucial for the anti-metastatic effect of anti-epidermal growth factor receptor antibodies. *Cancer Immunol. Immunother.* **2007**, *56*, 1701–1710. [CrossRef]
27. Garrido, G.; Rabasa, A.; Sanchez, B.; Lopez, M.V.; Blanco, R.; Lopez, A.; Hernandez, D.R.; Perez, R.; Fernandez, L.E. Induction of immunogenic apoptosis by blockade of epidermal growth factor receptor activation with a specific antibody. *J. Immunol.* **2011**, *187*, 4954–4966. [CrossRef]
28. De la Cruz-Lopez, K.G.; Castro-Munoz, L.J.; Reyes-Hernandez, D.O.; Garcia-Carranca, A.; Manzo-Merino, J. Lactate in the Regulation of Tumor Microenvironment and Therapeutic Approaches. *Front. Oncol.* **2019**, *9*, 1143. [CrossRef]
29. Neufert, C.; Becker, C.; Neurath, M.F. An inducible mouse model of colon carcinogenesis for the analysis of sporadic and inflammation-driven tumor progression. *Nat. Protoc.* **2007**, *2*, 1998–2004. [CrossRef]

30. Neufert, C.; Heichler, C.; Brabletz, T.; Scheibe, K.; Boonsanay, V.; Greten, F.R.; Neurath, M.F. Inducible mouse models of colon cancer for the analysis of sporadic and inflammation-driven tumor progression and lymph node metastasis. *Nat. Protoc.* **2021**, *16*, 61–85. [CrossRef]
31. Tanaka, T.; Kohno, H.; Suzuki, R.; Yamada, Y.; Sugie, S.; Mori, H. A novel inflammation-related mouse colon carcinogenesis model induced by azoxymethane and dextran sodium sulfate. *Cancer Sci.* **2003**, *94*, 965–973. [CrossRef] [PubMed]
32. Suzuki, R.; Kohno, H.; Sugie, S.; Nakagama, H.; Tanaka, T. Strain differences in the susceptibility to azoxymethane and dextran sodium sulfate-induced colon carcinogenesis in mice. *Carcinogenesis* **2006**, *27*, 162–169. [CrossRef] [PubMed]
33. Becker, C.; Fantini, M.C.; Wirtz, S.; Nikolaev, A.; Kiesslich, R.; Lehr, H.A.; Galle, P.R.; Neurath, M.F. In vivo imaging of colitis and colon cancer development in mice using high resolution chromoendoscopy. *Gut* **2005**, *54*, 950–954. [CrossRef] [PubMed]
34. Li, Y.; Park, J.S.; Deng, J.H.; Bai, Y. Cytochrome c oxidase subunit IV is essential for assembly and respiratory function of the enzyme complex. *J. Bioenerg. Biomembr.* **2006**, *38*, 283–291. [CrossRef]
35. Kadenbach, B.; Huttemann, M.; Arnold, S.; Lee, I.; Bender, E. Mitochondrial energy metabolism is regulated via nuclear-coded subunits of cytochrome c oxidase. *Free Radic. Biol. Med.* **2000**, *29*, 211–221. [CrossRef]
36. Zhao, Y.; Hu, X.; Liu, Y.; Dong, S.; Wen, Z.; He, W.; Zhang, S.; Huang, Q.; Shi, M. ROS signaling under metabolic stress: Cross-talk between AMPK and AKT pathway. *Mol. Cancer* **2017**, *16*, 79. [CrossRef]
37. Sünderhauf, A.; Hicken, M.; Schlichting, H.; Skibbe, K.; Ragab, M.; Raschdorf, A.; Hirose, M.; Schaffler, H.; Bokemeyer, A.; Bettenworth, D.; et al. Loss of Mucosal p32/gC1qR/HABP1 Triggers Energy Deficiency and Impairs Goblet Cell Differentiation in Ulcerative Colitis. *Cell. Mol. Gastroenterol. Hepatol.* **2021**, *12*, 229–250. [CrossRef]
38. Sünderhauf, A.; Raschdorf, A.; Hicken, M.; Schlichting, H.; Fetzer, F.; Brethack, A.K.; Perner, S.; Kemper, C.; Ghebrehiwet, B.; Sina, C.; et al. GC1qR Cleavage by Caspase-1 Drives Aerobic Glycolysis in Tumor Cells. *Front. Oncol.* **2020**, *10*, 575854. [CrossRef]
39. Sünderhauf, A.; Skibbe, K.; Preisker, S.; Ebbert, K.; Verschoor, A.; Karsten, C.M.; Kemper, C.; Huber-Lang, M.; Basic, M.; Bleich, A.; et al. Regulation of epithelial cell expressed C3 in the intestine—Relevance for the pathophysiology of inflammatory bowel disease? *Mol. Immunol.* **2017**, *90*, 227–238. [CrossRef]
40. Bronte, V.; Pittet, M.J. The spleen in local and systemic regulation of immunity. *Immunity* **2013**, *39*, 806–818. [CrossRef]
41. Sugihara, K.; Jass, J.R. Colorectal goblet cell sialomucin heterogeneity: Its relation to malignant disease. *J. Clin. Pathol.* **1986**, *39*, 1088–1095. [CrossRef]
42. Milosevic, V.; Vukmirovic, F.; Zindovic, M.; Krstic, M.; Milenkovic, S.; Jancic, S. Interplay between expression of leptin receptors and mucin histochemical aberrations in colorectal adenocarcinoma. *Rom. J. Morphol. Embryol.* **2015**, *56*, 709–716. [PubMed]
43. Kasprzak, A.; Seraszek-Jaros, A.; Jagielska, J.; Helak-Lapaj, C.; Siodla, E.; Szmeja, J.; Kaczmarek, E. The Histochemical Alterations of Mucin in Colorectal Carcinoma Quantified by Two Efficient Algorithms of Digital Image Analysis. *Int. J. Mol. Sci.* **2019**, *20*, 4580. [CrossRef] [PubMed]
44. Raschdorf, A.; Sunderhauf, A.; Skibbe, K.; Ghebrehiwet, B.; Peerschke, E.I.; Sina, C.; Derer, S. Heterozygous P32/C1QBP/HABP1 Polymorphism rs56014026 Reduces Mitochondrial Oxidative Phosphorylation and Is Expressed in Low-grade Colorectal Carcinomas. *Front. Oncol.* **2020**, *10*, 631592. [CrossRef] [PubMed]
45. Tajan, M.; Vousden, K.H. Dietary Approaches to Cancer Therapy. *Cancer Cell* **2020**, *37*, 767–785. [CrossRef] [PubMed]
46. Tannenbaum, A. The dependence of tumor formation on the composition of the calorie-restricted diet as well as on the degree of restriction. *Cancer Res.* **1945**, *5*, 616–625.
47. Ho, V.W.; Leung, K.; Hsu, A.; Luk, B.; Lai, J.; Shen, S.Y.; Minchinton, A.I.; Waterhouse, D.; Bally, M.B.; Lin, W.; et al. A low carbohydrate, high protein diet slows tumor growth and prevents cancer initiation. *Cancer Res.* **2011**, *71*, 4484–4493. [CrossRef]
48. Glaire, M.A.; Domingo, E.; Sveen, A.; Bruun, J.; Nesbakken, A.; Nicholson, G.; Novelli, M.; Lawson, K.; Oukrif, D.; Kildal, W.; et al. Tumour-infiltrating CD8(+) lymphocytes and colorectal cancer recurrence by tumour and nodal stage. *Br. J. Cancer* **2019**, *121*, 474–482. [CrossRef]
49. Galon, J.; Costes, A.; Sanchez-Cabo, F.; Kirilovsky, A.; Mlecnik, B.; Lagorce-Pages, C.; Tosolini, M.; Camus, M.; Berger, A.; Wind, P.; et al. Type, density, and location of immune cells within human colorectal tumors predict clinical outcome. *Science* **2006**, *313*, 1960–1964. [CrossRef]
50. Konjar, S.; Veldhoen, M. Dynamic Metabolic State of Tissue Resident CD8 T Cells. *Front. Immunol.* **2019**, *10*, 1683. [CrossRef]
51. Pardoll, D.M. The blockade of immune checkpoints in cancer immunotherapy. *Nat. Rev. Cancer* **2012**, *12*, 252–264. [CrossRef]
52. Topalian, S.L.; Taube, J.M.; Anders, R.A.; Pardoll, D.M. Mechanism-driven biomarkers to guide immune checkpoint blockade in cancer therapy. *Nat. Rev. Cancer* **2016**, *16*, 275–287. [CrossRef]
53. Zeboudj, L.; Maitre, M.; Guyonnet, L.; Laurans, L.; Joffre, J.; Lemarie, J.; Bourcier, S.; Nour-Eldine, W.; Guerin, C.; Friard, J.; et al. Selective EGF-Receptor Inhibition in CD4(+) T Cells Induces Anergy and Limits Atherosclerosis. *J. Am. Coll. Cardiol.* **2018**, *71*, 160–172. [CrossRef] [PubMed]
54. Derer, S.; Bauer, P.; Lohse, S.; Scheel, A.H.; Berger, S.; Kellner, C.; Peipp, M.; Valerius, T. Impact of epidermal growth factor receptor (EGFR) cell surface expression levels on effector mechanisms of EGFR antibodies. *J. Immunol.* **2012**, *189*, 5230–5239. [CrossRef] [PubMed]
55. Pirker, R.; Pereira, J.R.; von Pawel, J.; Krzakowski, M.; Ramlau, R.; Park, K.; de Marinis, F.; Eberhardt, W.E.; Paz-Ares, L.; Storkel, S.; et al. EGFR expression as a predictor of survival for first-line chemotherapy plus cetuximab in patients with advanced non-small-cell lung cancer: Analysis of data from the phase 3 FLEX study. *Lancet Oncol.* **2012**, *13*, 33–42. [CrossRef]

56. Lievre, A.; Bachet, J.B.; Boige, V.; Cayre, A.; Le Corre, D.; Buc, E.; Ychou, M.; Bouche, O.; Landi, B.; Louvet, C.; et al. KRAS mutations as an independent prognostic factor in patients with advanced colorectal cancer treated with cetuximab. *J. Clin. Oncol.* **2008**, *26*, 374–379. [CrossRef] [PubMed]
57. Allegra, C.J.; Jessup, J.M.; Somerfield, M.R.; Hamilton, S.R.; Hammond, E.H.; Hayes, D.F.; McAllister, P.K.; Morton, R.F.; Schilsky, R.L. American Society of Clinical Oncology provisional clinical opinion: Testing for KRAS gene mutations in patients with metastatic colorectal carcinoma to predict response to anti-epidermal growth factor receptor monoclonal antibody therapy. *J. Clin. Oncol.* **2009**, *27*, 2091–2096. [CrossRef]
58. Derer, S.; Berger, S.; Schlaeth, M.; Schneider-Merck, T.; Klausz, K.; Lohse, S.; Overdijk, M.B.; Dechant, M.; Kellner, C.; Nagelmeier, I.; et al. Oncogenic KRAS impairs EGFR antibodies' efficiency by C/EBPbeta-dependent suppression of EGFR expression. *Neoplasia* **2012**, *14*, 190–205. [CrossRef]
59. Kalantar-Zadeh, K.; Moore, L.W.; Tortorici, A.R.; Chou, J.A.; St-Jules, D.E.; Aoun, A.; Rojas-Bautista, V.; Tschida, A.K.; Rhee, C.M.; Shah, A.A.; et al. North American experience with Low protein diet for Non-dialysis-dependent chronic kidney disease. *BMC Nephrol.* **2016**, *17*, 90. [CrossRef]
60. Fouque, D.; Aparicio, M. Eleven reasons to control the protein intake of patients with chronic kidney disease. *Nat. Clin. Pract. Nephrol.* **2007**, *3*, 383–392. [CrossRef]
61. Ko, G.J.; Obi, Y.; Tortorici, A.R.; Kalantar-Zadeh, K. Dietary protein intake and chronic kidney disease. *Curr. Opin. Clin. Nutr. Metab. Care* **2017**, *20*, 77–85. [CrossRef] [PubMed]
62. Moskal, A.; Freisling, H.; Byrnes, G.; Assi, N.; Fahey, M.T.; Jenab, M.; Ferrari, P.; Tjonneland, A.; Petersen, K.E.; Dahm, C.C.; et al. Main nutrient patterns and colorectal cancer risk in the European Prospective Investigation into Cancer and Nutrition study. *Br. J. Cancer* **2016**, *115*, 1430–1440. [CrossRef] [PubMed]